ESA contract 18555

Development and production of Aeolus wind

Data products

TN 18.7 An assessment of Aeolus wind observations with the ECMWF model and preliminary Observing System Experiments

Authors

M. P. RENNIE
L. ISAKSEN
J. DE KLOE
G. MARSEILLE
A. STOFFELEN

CHANGE LOG

Version	Date	Comment
1.0	10/5/2019	First version following L. Isaksen review
1.1	8/8/2019	Updates following A. G. Straume review

Contents

1 Abstract

ESA's Aeolus mission has been demonstrated to be the first space-based Doppler Wind Lidar (DWL) technology that is fit for purpose, by providing acceptable quality wind observations. This conclusion was reached by comparing the Level-2B (L2B) horizontal line-of-sight (HLOS) wind observations to the ECMWF NWP model equivalents. It is also confirmed by the positive impact of Aeolus in some initial Observing System Experiments (OSEs).

The Commissioning Phase Aeolus L2B Rayleigh-clear HLOS wind (one-sigma) random errors were estimated to be typically 4.3 m/s and 3 m/s for Mie-cloudy HLOS winds, but with high variability depending on the signal levels which vary with meteorological conditions. The magnitude of the Mie HLOS wind noise is close to meeting the mission requirements in the free troposphere, however the Rayleigh noise is larger than the pre-launch mission requirements. The systematic errors (biases) are complex and vary with time, which is caused particularly by the larger than expected challenge in applying the weekly instrument calibrations and the zero wind ground returns along the orbit to correct for other bias sources. The sources of the biases are increasingly being characterised and understood, and it is expected that most of the bias will in future be corrected with the regular application of the instrument calibration in the on-ground data processing using the regular instrument response and ground return measurements — we provide evidence for this.

OSEs were done using the ECMWF data assimilation system for a forty-day period of the mission's Commissioning Phase (CP) when the systematic errors were reasonably stable with time. The impact of the data assimilation of Aeolus L2B HLOS winds on short range forecasts (up to 12 hours) is demonstrated to be mostly positive, via the generally statistically significant improvements in the forecast fit to other observation types sensitive to temperature, wind and humidity (such as radiosondes, aircraft and humidity sensitive microwave radiance observations). An exception to this is degradation in the lower stratospheric temperatures (relative to AMSU-A) which only occurs when the Rayleigh winds are being assimilated; the likely reason is related to the poor vertical resolution of the Rayleigh winds at these altitudes and the limitations of our observation operator (due to Commissioning Phase range-bin settings). The medium-range forecast impact shows positive signs in the Southern Hemisphere extratropics and tropics but did not reach statistical significance due to the relatively short forty-day test period. A longer period with well calibrated wind observations is required in future to confirm this. Overall, the impact on forecast skill is promising given the observation's biases, higher than expected noise levels and despite the relatively small size of the assimilated Aeolus dataset compared to other components of the observing system.

2 Introduction

Profiles of wind observations are the main component that is lacking in the Global Observing System according to the World Meteorological Organisation (WMO) Rolling Review of Requirements (WMO, 2018). There have been many studies highlighting the potential benefits of more wind profile observations for NWP; such as: Stoffelen et al. (2006), Marseille et al. (2008), Baker et al. (2014), Horányi (2015a), Tan et al. (2007), Weissman and Cardinalli (2007), Illingworth et al. (2018).

The European Space Agency's Aeolus satellite mission partially fills this gap and should confirm the value of wind profiles for NWP (Numerical Weather Prediction). Aeolus was launched on 22 August 2018 and is the first Doppler Wind Lidar (DWL) in space and the first European lidar in space.

Aeolus is an Earth Explorer mission which is part of the ESA's Living Planet Programme (Ingmann and Straume, 2016, www.esa.int/aeolus). The mission's main objective is to provide profiles of high-quality wind component observations from the surface up to the lower stratosphere,

using a DWL instrument (called Atmospheric LAser Doppler Instrument (ALADIN)) in a polar sun-synchronous, 320 km altitude, dawn-dusk orbit (18:00 local time equator crossing for the ascending node). The wind information consists of slant path profiles of the horizontal line-of-sight (HLOS) component, pointing in the direction perpendicular to the satellite-earth surface velocity vector. The mission lifetime is defined to be at least three years.

The ALADIN instrument is a powerful and highly frequency-stabilised pulsed ultraviolet (UV, 355 nm) DWL. The instrument laser emits powerful pulses of around 80 mJ at a frequency of 50 Hz through its 1.5 m telescope into the atmosphere. The light is scattered by air molecules (Rayleigh scattering), particles and hydrometeors (Mie scattering), and a very small fraction of the scattered light makes its way back to the instrument where it is received by the instrument's telescope. The backscattered signal is sampled in two channels; one for the backscatter from the clear-air molecules (a Double Fabry-Pérot spectrometer called the Rayleigh Channel) and one for the particulate backscatter (a Fizeau spectrometer called the Mie channel). The received signal is Doppler shifted (frequency shifted) due to the motion of the atmospheric scatterers along the instrument's field of view, which is determined by comparing the backscatter frequency to the instrument emit frequency. A detailed description of the mission can be found in ESA's ADM-Aeolus Science Report (ESA, 2008).

This paper is intended to provide a first look at the quality of the Commissioning Phase (hereafter abbreviated to CP) Aeolus data, and to provide guidance to other NWP centres and the scientific community on the usage of the Aeolus wind observations. In Section 4.1, the quality of the Aeolus Level-2B (L2B) HLOS wind observations is assessed for the first time, using the ECMWF global model as a reference. Short-range forecasts from NWP models have been used for decades to detect issues with observations e.g., Hollingsworth et al. (1986), Stoffelen (1999) and Lu et al. (2011). By applying this powerful method, we have also been able to detect many issues with the Aeolus data quality through comparing the Aeolus L2B HLOS winds to the ECMWF model equivalents.

We focus on data measured and processed during the Aeolus mission's CP, which lasted from late August 2018 until the end of January 2019, during which the Aeolus L2B winds were produced from 3 September 2018 until 14 January 2019[1]. During the CP, the L2B processing team (ECMWF and KNMI) collaborated closely with ESA and the Level-1 processing teams (DLR, DoRIT, Météo-France) in order to characterize, calibrate and validate the ALADIN instrument and the Aeolus data products. By comparing to the short-range forecast, anomalies were detected and reported, hence the expert teams could identify the root cause of many of the issues, whether they existed in the instrument or in the processing chain; all during a short time period of time. We describe some of the problems detected via NWP monitoring which are relevant for the scientific usage of Aeolus winds in NWP and for general scientific research. Further validation of the Aeolus data quality through comparisons with correlated observations from ground-based and airborne (remote sensing) instrumentation is performed by the Aeolus Calibration and Validation teams (CAL/VAL teams). The CAL/VAL teams also contain members comparing Aeolus observations directly to other wind observations available in the WMO Global Observing System (GOS), such as radiosondes, and to other NWP models from Meteorological Centres world-wide. In this way, the Aeolus observation quality can be well characterized through many sources, and it allows also NWP model errors (including biases) to be assessed. Other CAL/VAL teams also perform NWP impact assessments of Aeolus data using their weather models. The results of these validations are not further discussed here.

In Section 0, the results of the first assessment of the impact of Aeolus winds on NWP forecast skill is given. However, it should be noted that this is from a relatively short time period and hence the medium range forecast impact has not reached statistical significance. The reasons for choosing

---

[1] After which a satellite anomaly caused ALADIN to switch off until 15 February 2019.

the relatively short focus period will be explained later. Therefore, we refer to this investigation as an initial impact assessment, with the expectation that the impact is likely to increase and become more robust when the issues identified in this report have been resolved by improved Ground Segment processors (and reprocessed datasets) and by improved data assimilation methods for Aeolus.

3 Methods

3.1 Aeolus Level-2B wind data

Aeolus wind products are the result of a multiple stage ground processing chain. The different processing levels are described in detail in ESA (2008) and are also provided in the Algorithm Theoretical Baseline Documents for the various product levels (Level 1B and Level 2B) which are available here: https://earth.esa.int/aos/AeolusCalVal. The Aeolus L2B HLOS wind product contains observations suitable for use in NWP and scientific research, due to several important corrections which are applied relative to the Level-1B (L1B) HLOS wind products. The website: https://confluence.ecmwf.int/display/AEOL__provides the L2B processor software and its documentation for download. The Aeolus ground segment processing chain has been developed since the early 2000's by various entities including: ESA, Airbus DS, DLR, MDA, DoRIT, KNMI, Météo-France and ECMWF. Tan et al. (2008) explains the basics of the L2B processor, however this reference is partially obsolete due to several significant algorithm updates since then. The L2B processor Algorithm Theoretical Baseline Document is the most up-to-date description.

The L2B dataset used for this investigation is a combination of reprocessed data and data produced operationally by the Ground Segment in near-real time (NRT). All the data was produced with the L1B processor version 7.04 and L2B processor version 3.01[2]. The period from 3 September to 19 November 2018 used reprocessed data for which the L2B Earth Explorer (EE) product was generated by ESA's Payload Data Ground Segment (PDGS) for the use of the Aeolus CAL/VAL teams. The reprocessed L2B EE products were converted to BUFR products by the L2B team. For the NRT data, ECMWF's L2/Met PF (Level-2 Meteorological Processing Facility) provided the the L2B EE and corresponding BUFR data. The L2B BUFR data are primarily used by NWP centres as the means of getting the data into their data assimilation systems.

The L2B processor's settings determine many characteristics of the L2B wind observations. An important setting is the maximum horizontal averaging length-scale. For the CAL/VAL dataset this was set to one Basic Repeat Cycle (BRC) for both the Rayleigh and the Mie observations, meaning the HLOS winds are produced from up to 30 smaller horizontal-scale (~2.9 km) measurements, resulting in observations of up to approximately 87 km horizontal extent. The vertical resolution is not controlled by the L2B processor — the vertical range-bin settings were defined by ESA and commanded on-board the satellite, therefore the resolution cannot be further improved upon within the data ground processing. The vertical thickness of the 24-available range-bins typically varies and can be set from 250 m to 2 km in 250 m increments, nominally becoming thicker with height to result in winds with reasonable noise levels. The Mie and Rayleigh channels typically have different range-bin settings. The range-bin settings were kept fixed during nearly all the CP with settings chosen to ensure sufficient sampling of the surface (many 250 m bins near the surface). This is because backscatter signals from the ground provide a zero-wind reference, which is an important source of wind calibration, especially during the CP where it is useful to build up knowledge about Aeolus biases.

Out of the four available L2B wind observation types (Rayleigh-clear, Rayleigh-cloudy, Mie-

---

[2] The Payload Data Ground Segment (PDGS) baseline is 2B02.

clear, Mie-cloudy), we focus on the Rayleigh-clear and Mie-cloudy winds, as they are significantly better quality than the other two types. An example of Aeolus L2B HLOS wind observations (both L2B Rayleigh-clear and Mie-cloudy) from one orbit is shown in Figure 1. With one BRC averaging, there are around 5.5 times more Rayleigh-clear than Mie-cloudy winds. ALADIN's line-of-sight is perpendicular to the satellite orbit, and so it points mostly approximately 10 degrees off the zonal direction for most of the orbit. Therefore, the HLOS winds generally have more information on the zonal (u) wind component than to the meridional (v) wind component. However, near the poles ALADIN becomes more sensitive to the meridional (v) wind component, which is evident from the example coverage shown in Figure 2. Outside of polar regions, for ascending orbit phases Aeolus measures the westerly jet streams as positive HLOS winds, and for descending orbit phases the westerly jet streams are measured as negative HLOS winds. Areas with the strongest winds (jet streams) are annotated in Figure 1. Being an active space-borne optical instrument, ALADIN cannot observe below optically thick clouds, hence there are areas with no observations (near the surface) which are indicated in black.
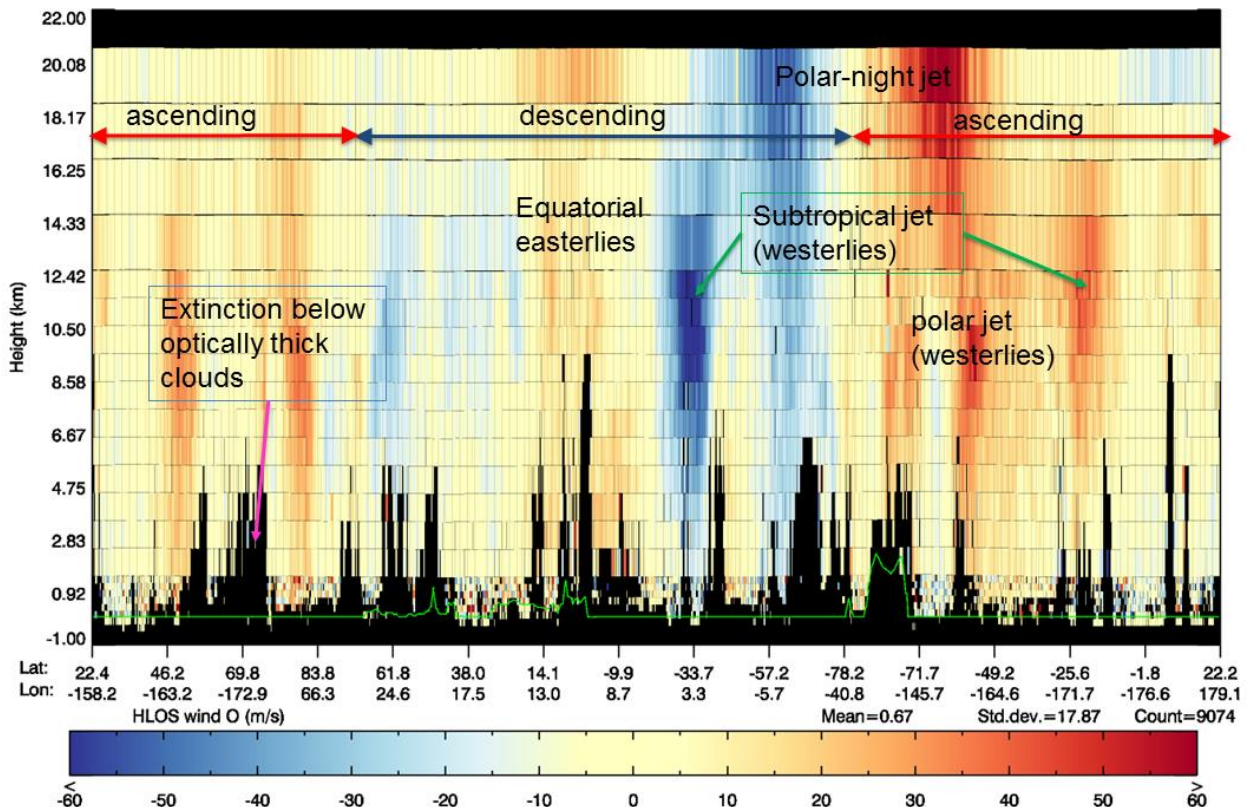
Figure 1. L2B Rayleigh-clear and Mie-cloudy HLOS wind observations for one orbit on 15 September 2018. The vertical axis is the geometric height relative to EGM96 geoid and the horizontal axis is the time along the orbit (but is labelled by latitude/longitude geolocations along the orbit). The colours indicate the HLOS wind speed. To more clearly show lower wind speeds, the scale saturates at ±60 m/s (despite the speed in some of the jet streams reaching larger values). Black areas indicate an absence of observations. Each observation is plotted as a coloured rectangle indicating the spatial limits of the observation, hence the vertical sampling (range-bin settings) can be seen (the horizontal extents are hard to see in this whole orbit plot). The Digital Elevation Model i.e. Earth's surface is shown in green.

Figure 2. An example of Aeolus near surface geolocations in one day. The line-of-sight pointing of ALADIN is indicated by the purple arrows for an ascending (Eastwards) and descending (Westwards) orbit. The higher spatial sampling near the north pole is evident.

The vertical range-bin settings (RBS)[3] that was applied in the CP is evident in Figure 1. The RBS varied from 250 m near the surface to 2 km thick in the lower stratosphere, and reached a maximum altitude of around 20 km. The near-surface 250 m range-bins are too thin to provide enough signal for good quality Rayleigh winds, but the Mie winds are good, due to relatively large backscatter from the top of clouds.

In the retrieval of HLOS wind observations, calibration information on how the Rayleigh and Mie spectrometer instrument responses change with frequency is required (ESA, 2008). To well characterize and quantify the different contributors to the Aeolus instrument drift, to verify the satellite Attitude and Orbital Control Systems (AOCS) and the calculations of the satellite attitude, the CAL/VAL dataset was generated from a fixed set of instrument response calibration files. However, weekly calibration procedures were performed during the CP and will continue to be performed during the mission lifetime. Another source of calibration is ground return winds which can be used to correct for possible satellite misspointing, thermal and range dependencies, which can lead to height dependent and short (within an orbit) and long (seasonal effects) term biases. After analysis and quality control of the weekly response calibrations, ground returns and L2B data quality and after improvements in the calibration ground processing algorithms have been found this information will be applied in the data processing in NRT for new data and in future reprocessing activities for historical data i.e. when a calibration strategy has been defined.

. The calibration for the L2B processor Rayleigh winds is provided via a file called the Rayleigh-Brillouin Correction look-up table (AUX_RBC_L2 file) which is produced by the Aeolus Calibration Suite software. For the CAL/VAL dataset the AUX_RBC_L2 was derived from an Instrument Spectral Response (ISR) (ESA, 2008) measured on 19 September 2018; an Instrument Response Calibration (IRC) was not directly used (via the so-called update Corrected Spectral Registration (CSR) procedure, which is part of the Aeolus Calibration Suite data processing software). This was because testing using the IRC led to significantly biased winds (e.g. -7 m/s) when applying it to the update CSR software (version available at the time).

To account for an observed frequency offset between the internal reference and atmospheric path response curves as seen in the Rayleigh Response Calibration (RRC) after the instrument was launched, the atmospheric response curves had to be shifted by approximately 160 MHz in the

---

[3] Vertical range-bin sampling more suitable for NWP exploitation has been applied since 26 February 2019.

AUX_RBC_L2 file produced by the Aeolus Calibration Suite. The resulting updated AUX_RBC_L2 file was used in the L2B wind processing, but this led to an almost constant global bias of several m/s with respect to ECMWF model equivalent HLOS winds during the September 2018 period. Hence, it was decided, as a preliminary measure, to adjust the frequency shift such that the L2B Rayleigh-clear global mean departures with respect to ECMWF's short-range forecast became close to zero in that period, which was achieved by changing the shift to 155.4 MHz. This tuning, using global ECMWF statistics, was not ideal but was deemed to be necessary in this very early phase of the mission to get an early dataset suitable for impact studies. It should be noted that the ECMWF short-range forecast has small global and regionally averaged wind bias compared to high quality observations such as radiosondes (e.g. less than 0.3 m/s for zonal wind component). More recently (in February/March 2019), several improvements in the Rayleigh calibration processing were found, so that tuning to the ECMWF model was no longer required.

The applied L2B processor Mie wind calibration information (the Mie Response Calibration (MRC)) is the same as that used by the Level-1B product Mie wind observations. It was chosen by the L1 experts based on assessments of the quality of the weekly MRCs (based on ground returns over Antarctica in nadir pointing mode). A MRC valid on 15 October 2018 was chosen and applied in the processing/re-processing of the whole CP dataset. Nominally the L2Bp obtains the MRC information from the L1B wind mode product, but in an offline testing mode it is possible to read the MRC information directly (from AUX_MRC_1B file). Testing showed that it is possible to tune the MRC parameters to minimise the Mie wind bias with respect to the ECMWF model, in a similar way to that done for the Rayleigh winds, however because the Mie bias was not very large, it was not done to avoid a possible risk of introduction NWP model biases into the satellite observation dataset.

3.2 Observation-minus-background departure statistics

As discussed in Section 2, the assessment of the quality of the L2B HLOS wind observations versus a state-of-the-art data assimilation system is a very powerful method. We have used the ECMWF short-range forecast model equivalent HLOS winds to compute observation-minus-background (O-B) departure statistics. The ECMWF background forecasts are of course not the truth, otherwise there would be no point to Aeolus, but over large spatial scales or large time averages they have a good level of accuracy. We have reasonable estimates of the magnitude of the forecast wind errors via O-B statistics for high quality measurements (such as radiosonde winds), and of their spatial distribution and correlations via ECMWF's Ensemble of Data Assimilations (EDA, Isaksen et al., 2011) spread.

Our applied HLOS wind observation operator is:

$$v_{HLOS} = -u \sin \theta - v \cos \theta$$

That is, HLOS wind is a linear function of the NWP model zonal wind component (*u*) and meridional wind component (*v*) interpolated to the geolocation of the Aeolus observation. θ is the azimuth angle, provided as part of the observation geolocation. This observation operator assumes that the vertical wind component is negligible, which may be a poor assumption in certain conditions e.g. backscatter in areas of vertical motion e.g. associated with convection. However, it should be noted that most of the vertical motion associated with strongly convective cloud systems occurs inside the clouds, and that the Aeolus signal is quickly attenuated in the first few 10ths of meters of such clouds. Furthermore, wind observations in areas with Clear Air Turbulence (CAT) or in regions of turbulent in-flow to convective clouds systems may contain a significant vertical wind component. The impact of vertical motion on the Aeolus HLOS winds will be investigated further in future scientific studies.

The ECMWF model equivalent HLOS wind is derived from the model u and v components after they have been interpolated to the observation's centre-of-gravity geolocation point, rather than a more realistic averaging of the model state horizontally and vertically over the observed volume. The point observation operator is thought to be a reasonable approximation in the horizontal given

that the effective resolution of ECMWF's global model is in reasonable agreement with the horizontal resolution of L2B winds (Saleh's paper). However, vertically it is a poorer assumption given the model's vertical shear often varies significantly over the possible 1-2 km range-bins of Aeolus. It will be investigated in the future if a more representative forward model (e.g. accounting for the molecular attenuated backscatter variation in the range-bin for the Rayleigh channel; a solution for the Mie is less obvious) can reduce forward model error and hence improve impact, particularly in strong vertical wind shear conditions. A more complete forward model would assimilate L1B useful signal levels and hence use the full lidar equation, but this can easily become very complicated (and instrument calibration dependent), probably without much benefit. Alternatively, finer RBS can alleviate this issue.

Two methods were used to calculate O-B statistics for this study. The first is an unorthodox method, using the Aeolus auxiliary meteorological file AUX_MET_12 file (shortened to AUX_MET in the rest of the paper). The AUX_MET contains vertical profiles of ECMWF operational model fields along Aeolus' predicted ground-track geolocations (T$_{CO}$ 1279 model trajectory, sampled every 3 seconds (~22 km) along predicted orbit). The AUX_MET is a necessary input for the L2B processor to perform the Rayleigh-Brillouin Correction (Dabas, 2008), using a priori information model temperature and pressure. The AUX_MET also provides wind u and v wind components (for diagnostics, i.e. are not used in the L2Bp wind retrieval) as a function of geometric altitude, which can be forward modelled to HLOS wind. Therefore, the AUX_MET provides a convenient and co-located wind reference to perform O-B statistics. Since the AUX_MET data is already interpolated to the predicted ground-track of Aeolus, the nearest-neighbour winds from the AUX_MET data is used for the departure statistics. The AUX_MET data provides up to 30-hour forecasts, however the O-B statistics are restricted to use the 0-20 hour forecast range because shorter forecasts provide a more accurate reference.

The AUX_MET O-B statistics are calculated and plotted via bespoke Aeolus monitoring tools that have been developed over several years using simulated datasets (Rennie, 2016). The method is suited to small datasets e.g. up to one day's data. To avoid outliers strongly affecting the non-robust metrics e.g. mean and standard deviation, some quality control (QC) is needed. The QC is based on the L2Bp estimated HLOS wind error, which is derived using the useful signal amplitudes. No model short-range forecast-based QC, i.e. first-guess check, is required for this method. Thresholds of estimated errors of 8 m/s for the Rayleigh-clear and 4 m/s for the Mie-cloudy, respectively, were found to remove most outliers (gross errors) without rejecting too large a fraction of observations. For the Rayleigh observations, we discard 250 m thick range-bin data from the statistics, since they are so noisy that they are effectively unusable.

A more traditional method of deriving O-B statistics at ECMWF was also used. Here the Aeolus L2B BUFR data is ingested into the ECMWF data assimilation system and the O-B and O-A (observation-minus-analysis) departure statistics are calculated as described in Section 3.3.1. In such monitoring experiments Aeolus was blacklisted, i.e., the data is not given any weight in the assimilation. The model is run at a lower than operational horizontal resolution T$_{CO}$399 (~29 km) to save computational costs and running time (without too significant a loss in model resolution). ECMWF's generic observation monitoring software is then used to calculate the statistics, which can handle very large datasets e.g. several months of data for generating time-series plots. The QC can optionally use a model background (first-guess) check an also threshold check on the L2Bp estimated HLOS wind standard error. The model background check rejects observations for which the O-B departure is greater than five times the expectation, estimated by $\sqrt{\sigma_O^2 + \sigma_B^2}$, and is aimed at removing outliers (Järvinen and Andersson, 1999). With the first-guess check applied, the L2Bp estimated error thresholds could be relaxed relative to the AUX_MET O-B method e.g. 12 m/s for the Rayleigh-clear and 4 m/s for the Mie-cloudy were chosen.

3.3 Observing system experiments

Initial NWP impact assessment of Aeolus L2B HLOS winds was done by observing system experiments (OSE). OSEs are necessary to reliably assess the forecast impact in the medium range.

3.3.1 Further information on the Aeolus observation operator

Preparatory steps for the Aeolus observation operator are made using standard ECMWF data assimilation procedures. The L2B vertical centre-of-gravity geometric heights (with respect to EGM96 geoid) are converted to an equivalent atmospheric pressure, using the background forecast. First the geometric heights are converted to geopotential using a normal gravity formula (Somigliana's equation), then the geopotential is converted to pressure (using standard ECMWF data assimilation conversions, see ECMWF, 2018). It would be more correct to forward model the geometric heights on model levels and then to interpolate the model winds to Aeolus as a function of geometric height, however the improvement from this is expected to be small. An advantage of having pressure as the vertical coordinate is that other wind observations (e.g. radiosondes, aircraft, Atmospheric Motion Vectors) are also assimilated as a function of pressure and Aeolus can therefore be easily compared to them.

In the next step, vertical profiles of model wind components are horizontally interpolated to the geolocation of the L2B observation (centre-of-gravity latitude and longitude). The model u and v components are vertically interpolated (linear in the logarithm of pressure) to the assigned pressure and the HLOS wind formula (see Section 3.2) is applied as if the observation is a point-like wind.

3.3.2 Observing system experiment set-up

The OSE control run uses the ECMWF model at cycle 45r1 (which was used in the ECMWF operational configuration from June 2018 to June 2019), with the 4D-Var outer loop horizontal resolution at $T_{CO}511$ (23 km grid spacing), inner loops at T_{CO} 255/319/399 with 137 vertical levels up to 80 km. The nominal ECMWF operational set of satellite and conventional observations is assimilated. The focus period for the OSE is from 12 September 2018 until 16 October 2018, which was chosen because it was a period during which systematic errors in the L2B dataset were relatively stable with time and the instrument health was good (see Section 4.1 on O-B time series monitoring results). However, the OSE was performed for the whole of the CP to see the impact.

The experiments are the same as the control, except that they additionally assimilate the Aeolus L2B HLOS wind observations (via the L2B BUFR product). Two experiments were performed; one assimilating both the Rayleigh-clear and the Mie-cloudy observations and one assimilating only the Mie-cloudy observations, to determine the relative importance for NWP impact of each observation type.

The assigned Aeolus observation errors are based on the L2Bp estimated observation errors. The L2Bp estimated errors correlate well with the O-B standard deviation (as demonstrated in Sections 4.1.1 and 4.1.2), but they appear to be underestimated due to being only an instrument precision estimate, considering only shot-noise; they do not include model representativeness error. It was decided to scale the L2Bp estimated errors by 1.5 for the Mie-cloudy and 1.1 for the Rayleigh-clear (based on experience from pre-launch simulation studies). More recent testing suggests 1.4 to be more optimal for the Rayleigh winds.

3.3.3 Quality control decisions and corrections

Being the first few months of data from a new observation type, there are various extra (non-nominal)

corrections and quality control (QC) decisions that were applied (based on the available data quality analysis) to try to maximise the available data. The applied QC and corrections were done before the data assimilation, but after the BUFR data is read into the ECMWF data assimilation system. The QC decisions and data corrections included:

- Only the Rayleigh-clear and Mie-cloudy winds are assimilated (i.e., Rayleigh-cloudy and Mie-clear are rejected due to their generally poorer quality).
- Observations with assigned observation errors (i.e. after scaling) greater than a threshold were rejected with the aim of removing gross errors without rejecting too many good observations (this requires more refined tuning in the future):
  - Rayleigh-clear:
    - if pressure < 90 hPa, reject if assigned observation error > 11 m/s
    - if 90 <pressure<200 hPa, reject if assigned observation error > 7.7 m/s
    - if pressure > 200 hPa, reject if assigned observation error > 6.6 m/s
  - Mie-cloudy: reject if assigned observation error > 4.5 m/s
- The HLOS wind observation geometric heights were corrected by adding 250 m. This was required due to a known error in the LOS (Line of Sight) pointing knowledge during the CP (star-tracker calibration issue).[4]
- The Mie-cloudy winds were bias corrected by -1.35 m/s (global constant offset) to make them agree (in the global average) with the ECMWF model winds (this correction is only appropriate for the Aeolus data for the 12 September to 16 October 2018 period). The ECMWF model has biases less than 0.3 m/s on average (compared to radiosondes). The Mie bias is thought to be have been caused by imperfect calibration e.g. noise during the calibration procedure or errors in the processing algorithms.
- Specific pressure ranges for the Rayleigh channel were blacklisted to try to avoid biased HLOS winds that occur for specific range-bins (which was caused by so-called "hot" pixels, see the further explanation in Section 4.1.1). This method worked reasonably well, but was found to be imperfect, due to the difficulty of fixed altitude range-bins varying in pressure along the orbit. The blacklisting performed was for:
  - Rayleigh-clear:
    - Avoid range-bin 11 by rejecting data between 400-500 hPa for the whole period
    - Avoid range-bin 5 by rejecting data between 150-200 hPa after 4/11/2018
    - Avoid range-bin 15 by rejecting data between 700-800 hPa after 24/11/2018
  - Mie-cloudy:
    - Avoid range-bin 13 by rejecting data between 600-750 hPa after 21/10/2018
- Winds within 20 hPa (around 160 m) of the model orography were discarded because occasionally ground returns are wrongly classified as wind observations.
- Rayleigh winds with range-bin thicknesses of 250 m were rejected due to excessive noise.
- Rayleigh winds with horizontal accumulation lengths less than 60 km and Mie less than 5 km were rejected to try to avoid outliers.
- Specific periods when the satellite switched from star-tracker A to B were blacklisted, because the lack of consistent star-tracker calibration during CP caused very large wind biases. The blacklisting:

---

[4] This error was resolved on 26 February 2019 in operational data.

- o Data from 03:00 UTC on 25/9/2018 until 26/9/2018 14:51 UTC
- o Data from 9/11/2018 between 09:25 UTC and 15:25 UTC
- A method was employed to avoid duplicate observations that are present from overlaps between orbital dumps.

No spatial thinning of the observations was applied; this will be investigated in the future. As mentioned in Section 2.2, a 5-sigma background forecast departure check is applied.
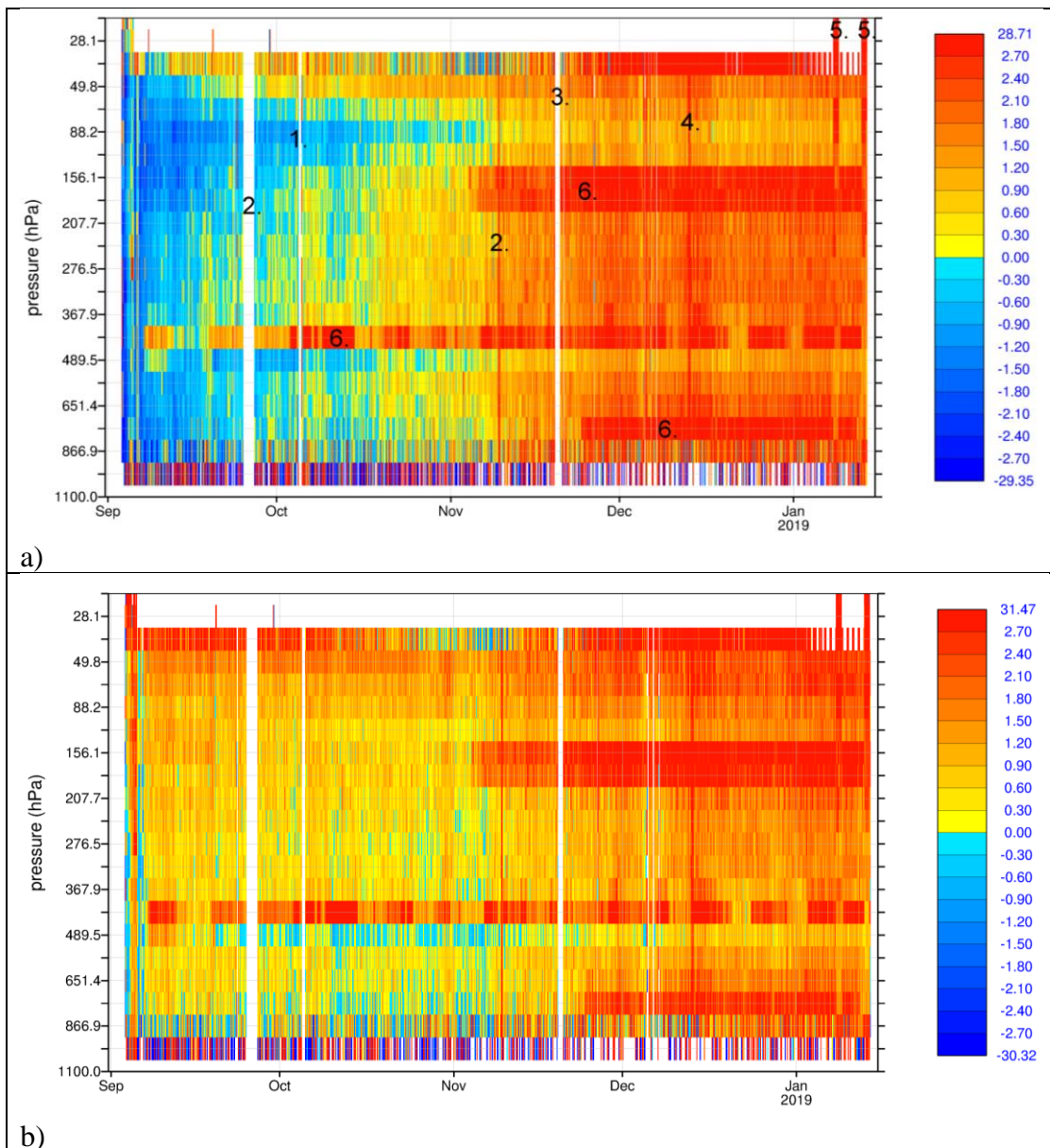
After QC there were typically 40,000-50,000 HLOS winds assimilated per 12 hours during the focus period. This is effectively ~8% the number of Atmospheric Motion Vector (AMV) winds assimilated per 12 hours (600,000 wind components). Aeolus provided only around 0.2% of the total number of observations assimilated in this OSE.

4 Results

4.1 O-B monitoring statistics

4.1.1 Rayleigh-clear HLOS wind O-B time variations and anomalies

The precision and accuracy of the L2B HLOS winds depends on many factors such as: signal levels; calibration quality; L2Bp algorithms and quality control decisions. It is outside the scope of this paper to investigate in detail the instrumental reasons for the levels of precision and accuracy found for Aeolus data. Via the assimilation experiment in which the Aeolus L2B is blacklisted, but departures are still calculated (see Section 3.2), time-series of O-B statistics were calculated. Figure 3 shows the L2B Rayleigh-clear HLOS wind global statistics of mean O-B binned by time (in 3 hourly slots) and pressure (pressure bins chosen so that the pressure axis is linearly proportional to altitude). The mean of O-B was found to depend on whether the satellite is in the ascending or descending phase of its polar orbit, hence the statistics are split accordingly in Figure 3 a) and b).

a)

b)

Figure 3. Global mean(O-B) as a function of time (every 3 hours) and pressure (a selection of pressure ranges) for the L2B Rayleigh-clear HLOS winds. The colour-scale has units of m/s. a) Ascending orbit phases and b) descending orbit phases. Numbered features in a) are referred to in the text.

Some anomalies and outages of the data are identified via the annotated numbers in Figure 3 a). The associated causes are listed below:
1. Satellite on-board software anomaly period
2. Star-tracker problem periods
3. Data gap due to a transition from reprocessed to operationally produced BUFR data
4. Flight model A laser cold plate temperature test period
5. Testing of different vertical range-bin settings
6. Range-bins affected by enhanced dark current in memory zone pixels ("hot" pixels)

In both ascending and descending orbit phases, there is a clear positive trend in the mean of O-B with time. No evidence was found to suggest that the ECMWF background forecast winds are biased in this way, therefore it is concluded to be due to L2B HLOS wind systematic errors. There are differences in bias between ascending and descending phases, e.g., in September 2018 the ascending phase is negatively biased whereas the descending phase is positively biased. This was found to be at least partially due to HLOS wind speed dependent bias resulting from imperfect L2Bp Rayleigh calibration (see Section 4.1.3.1). The ascending orbit phases measure on average positive HLOS winds and descending phases measure on average negative HLOS winds, due to the prevalence of westerly zonal winds in the extratropics. Therefore, a HLOS wind speed dependent bias (slow bias) manifests itself also as differences in bias between ascending (negative bias) and descending phases (positive bias). More recent testing using the calibration information applicable at the time (Rayleigh Response Calibration in mid-September 2018) resulted in a smaller wind speed dependent bias (linear slope error reduced by ~2%, corresponding to 1 m/s reduction in bias for a 50 m/s HLOS wind).

O-B statistics showed wind biases associated with specific vertical range-bins. This led the L1B processor team to discover an unexpected instrument problem, which we refer to as "hot" pixels. Increased dark current background and noise levels were found on specific pixels of the instrument's Accumulation Charge-Coupled Device (ACCD). This is thought to be triggered due to space environment radiation exposure (personal communication with ESA). The small changes in dark current background levels are enough to cause range-bin dependent wind biases, particularly for the Rayleigh channel. Hot pixel induced wind bias tends to fluctuate with time as the level of dark current varies, apparently randomly. The pattern mostly seen is that the dark current levels raises to a very high level when the event is triggered, for then to fluctuate and stabilize after a while at a low elevation level. Some pixels however take a long time to stabilize or keep on fluctuating. The positive bias associated with range-bin 11 (~400 hPa) during this period was caused by a hot pixel showing particularly strong fluctuations, as can be seen in Figure 3. At the time of writing, it is planned in the next round of ground segment processor updates to use regular dark current calibration information to correct for this effect.

Figure 4 shows the global L2B Rayleigh-clear standard deviation of O-B as a function of time and pressure. This gives an impression of the observation random error changes, because the model short-range forecast errors are relatively stable with time. We show only the ascending orbit phase statistics, because the descending phase statistics are very similar. The random errors are very large near the surface because of the narrow 250 m range-bins, which results in low signal levels. The lowest standard deviations occur for range-bins around the 100 hPa level (~13-16 km). This is because of the switch to 2 km thick range-bins around this pressure level, as compared to the 1 km thick-range-bins at levels below (see Figure 1). Doubling the range-bin thickness should reduce noise

by roughly 40%, but at the cost of a significant loss in vertical resolution. The mid-tropospheric 1 km range-bins typically have O-B standard deviations of 4-5 m/s.

There is a general trend for increased standard deviation with time, particularly at the upper levels, e.g., at 200 hPa from late November onwards. This is assumed to be caused mainly by a combination of increased solar background noise affecting the southern hemispheric observations (as the polar summer approached) and due to a decrease in the FM-A laser UV output energy with time (ESA, personal communication). The random errors are steadier for the mid-tropospheric levels than for higher altitudes. Higher altitudes have much less signal due to the exponential decaying atmospheric density with height. Testing showed that the upper range-bin random error increase is strongly related to increasingly poor L2Bp classification of measurement-level data into clear and cloudy conditions because of increasingly noisy L1B measurement-bin scattering ratios associated with the decreasing laser energy. An improvement in the standard deviation is evident in the last few days of Figure 4. This is due to a change in the L2B processor settings which improved the clear-cloudy classification.
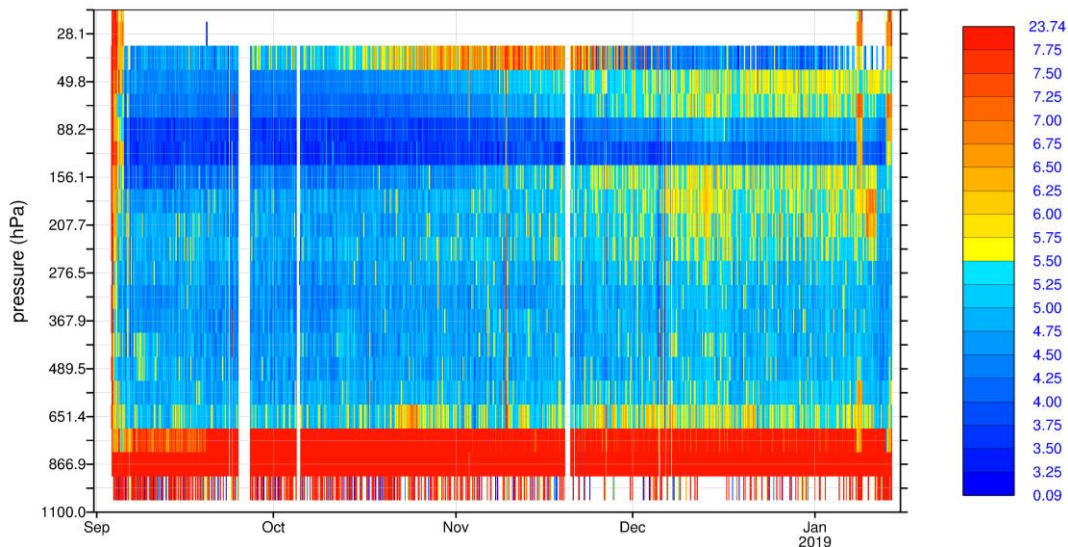

Figure 4. Global standard deviation(O-B) as a function of time (every 3 hours) and pressure for the L2B Rayleigh-clear HLOS winds. The scale has units of m/s. Data for ascending orbit phases only.

Figure 5 shows the ascending phase L2B Rayleigh-clear O-B statistics versus time for a mid-tropospheric pressure range (319-368 hPa, ~8 km) which is not affected by any hot pixel induced bias. The statistics are split into a) Northern Hemisphere (NH) extratropics and b) Southern Hemisphere (SH) extratropics. This pressure range is roughly where the Rayleigh winds achieve their best precision with 1 km thick range-bins, taking account of lower signal at lower altitudes due to cloud attenuation. A quantitative assessment of the bias and random error changes with time can be deduced from Figure 5. The bias increase with time, as already mentioned, is evident in Figure 5. The bias settles in early December 2018, but to different levels in the NH and the SH; 2-3 m/s in the NH and 1 m/s in the SH. After an initial decrease with time, the standard deviation of O-B is reasonably steady in the NH after October 2018, hovering around the 4.2 m/s level. The initial decrease is thought to be a combination of the decrease in the satellite to observation distance (range) as the satellite reached its final orbit and because the solar background noise reduced as the boreal winter approached. The standard deviation of O-B in the SH increases a little with time; probably due to a combination of decreasing UV laser energy and increasing solar background noise as the austral summer approaches.

Generally, the L2Bp estimated error (green lines of Figure 5) mirrors the changes in the O-B

standard deviation which suggests it is a useful estimate. The Rayleigh HLOS wind errors are significantly larger than the typical 1.5-2 m/s ECMWF background forecast errors, hence the standard deviation of O-B is dominated by the Rayleigh observation error. Note that for the SH plot, the L2Bp estimated observation error appears to be too large for increased solar background conditions in late November onwards i.e.it exceeds the standard deviation of O-B. This discrepancy should be investigated in future.
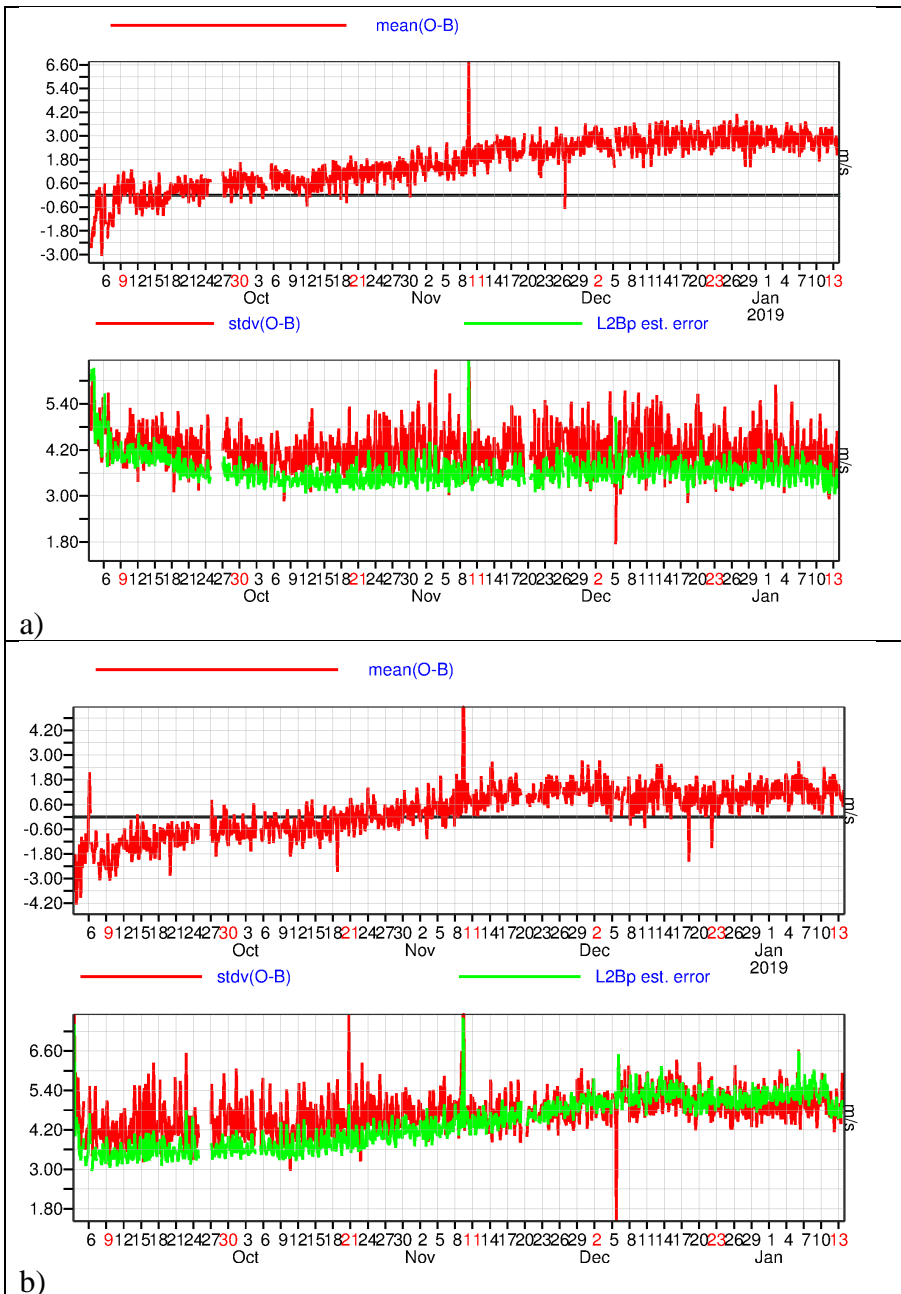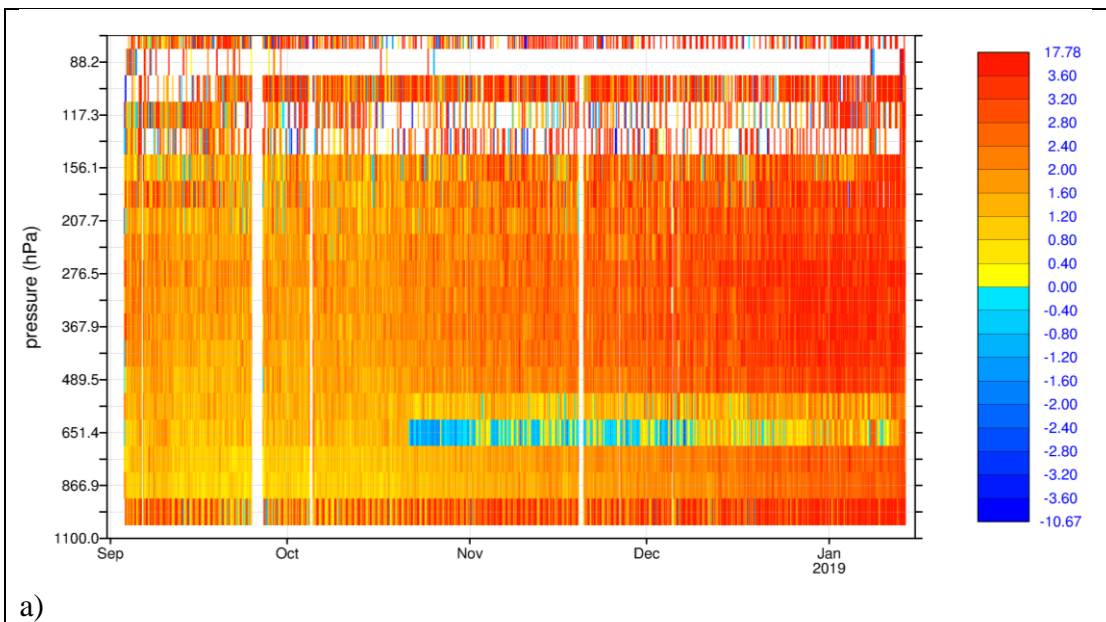

Figure 5. Time series (every 3 hours) of L2B Rayleigh-clear HLOS wind mean(O-B) (upper plot of each figure) and stdev(O-B) (lower plot of each figure) for the pressure range 319-368 hPa for ascending orbit phases only. a) Northern hemisphere extratropics (20-90 degrees latitude) b) southern hemisphere extratropics (-20 to -90 degrees latitude). The green line is the L2B processor estimated error derived from signal levels assuming shot-noise.

Early mission bias and random error fluctuations appear to settle by 12 September 2018, hence this is the chosen start date for the OSE focus period. In the NH, the biases reach significant levels

around 16 October 2018, hence the chosen end date for the focus period (Section 3.3.2). In the SH the bias also increases with time, but with a smaller rate. The OSE chosen dates are also appropriate for the Mie winds as shown in the next section.

4.1.2 Mie-cloudy HLOS wind O-B time variations and anomalies

Figure 6 shows the L2B Mie-cloudy HLOS wind mean O-B statistics, split into ascending (a) and descending (b) orbit phases. The Mie winds are affected by the same instrument and/or operations anomalies illustrated by the numbers 1-5 in Figure 3a, but these are not indicated again here. For both ascending and descending orbits there is a general positive trend in the bias with time (as also seen for the Rayleigh), but starting from an already small positive bias in September (since there was no tuning to the ECMWF model for the Mie calibration). The descending phases are slightly less positively biased than the ascending, with the difference in September suggesting the Mie winds have a fast wind speed dependent bias with respect to the model, in contrast to the Rayleigh which had a slow bias for this period (this is confirmed in Section 4.1.3). A standout feature from Figure 6 is the appearance of negatively biased winds for observations at ~650 hPa from 21 October 2018 onwards. This was due to a hot pixel affecting Mie range-bin 13.
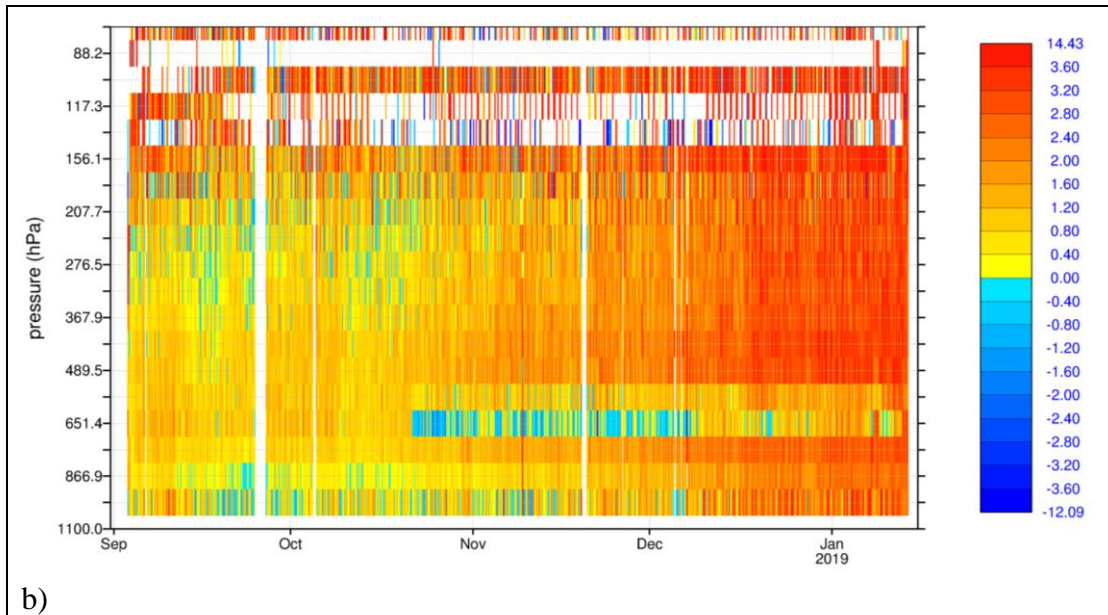

a)

18

	TN 18.7	Ref: AE-TN-ECMWF-GS-187
	An assessment of Aeolus wind observations with the	Version: 1.1
aeolus	ECMWF model and preliminary Observing System	Date: 8 August 2019
	Experiments	

b)

Figure 6. **Global mean(O-B) as a function of time (every 4 hours) and pressure for the L2B Mie-cloudy HLOS winds (CAL/VAL dataset). The scale has units of m/s. a) Ascending orbit phases and b)) descending orbit phases.**

Figure 7 shows the global L2B Mie-cloudy standard deviation of O-B as a function of time and pressure. Only ascending orbit phases are shown because the descending was very similar. As expected, the Mie winds have higher precision than the Rayleigh, by comparing to Figure 4 (note the colour scales are different). The standard deviations are smallest for the range-bins in the lower troposphere (which are 250 m range-bins with strong backscatter from optically thick boundary layer clouds). The very lowest range-bins are contaminated by ground return signals, hence the larger noise (resolved in the next L2B processor version, v3.10). There is an obvious increase in standard deviation associated with range-bin 13's hot pixel which shows up at ~600-650 hPa. Apart from the hot pixel influence there is not a clear trend in the standard deviation with time.
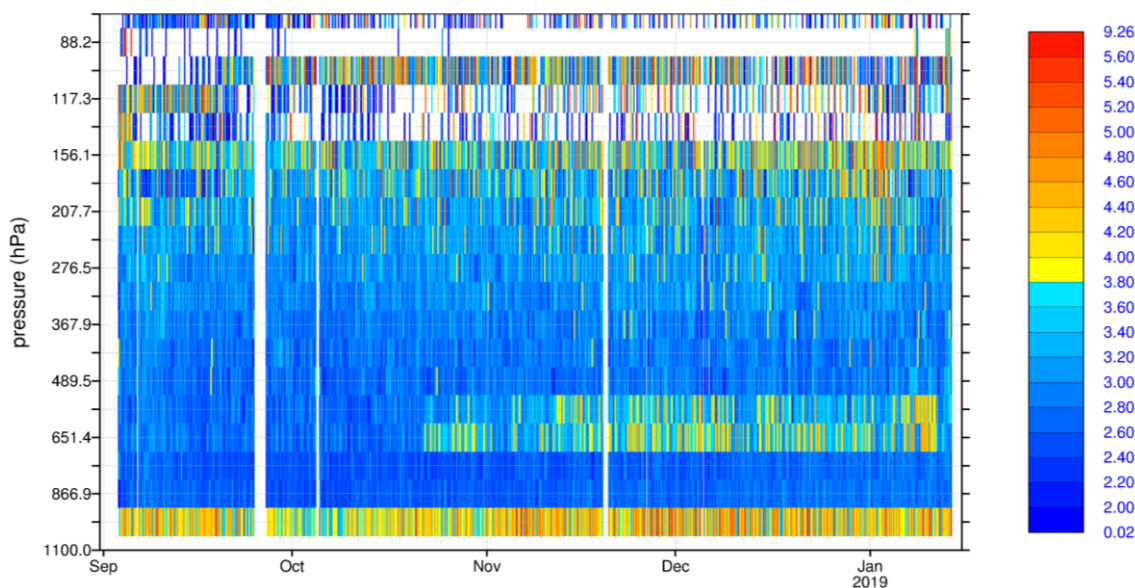

Figure 7. **Global standard deviation(O-B) as a function of time (every 4 hours) and pressure for the L2B Mie-cloudy HLOS winds. The scale has units of m/s. Data for ascending orbit phases only.**

Figure 8 shows the statistics for a pressure range in the lower troposphere (752-867 hPa, approximately 2 km altitude) which has a large sample of Mie winds resulting from strong backscatter off planetary boundary layer (PBL) cloud tops (and some aerosol); the figure is split into a) SH extratropics and b) NH extratropics (data for descending orbit phases only). This pressure range was not affected by hot pixels. It is evident that biases started to increase from early October in the NH, but much later in the SH; around late November. Bias settled in January to ~3 m/s in the NH and ~2 m/s in the SH. This behaviour has some similarities with the Rayleigh development, but the details differ. The random error in the NH shows a slight increase with time (which is not understood but may be due to seasonal changes in cloud conditions). In the SH the standard deviation of O-B is steady, which is promising for the mission given that the reported laser energy was around 20% lower in January 2019 than in September 2018. This suggests that the backscatter from clouds is sufficiently strong, such that the lower laser energy is not the limiting factor for the Mie random error. The magnitude and trends in L2Bp Mie estimated errors (green lines) correlates well with the standard deviation in O-B (red lines); suggesting it is a useful error estimate. Similar behaviour is found for other pressure ranges.
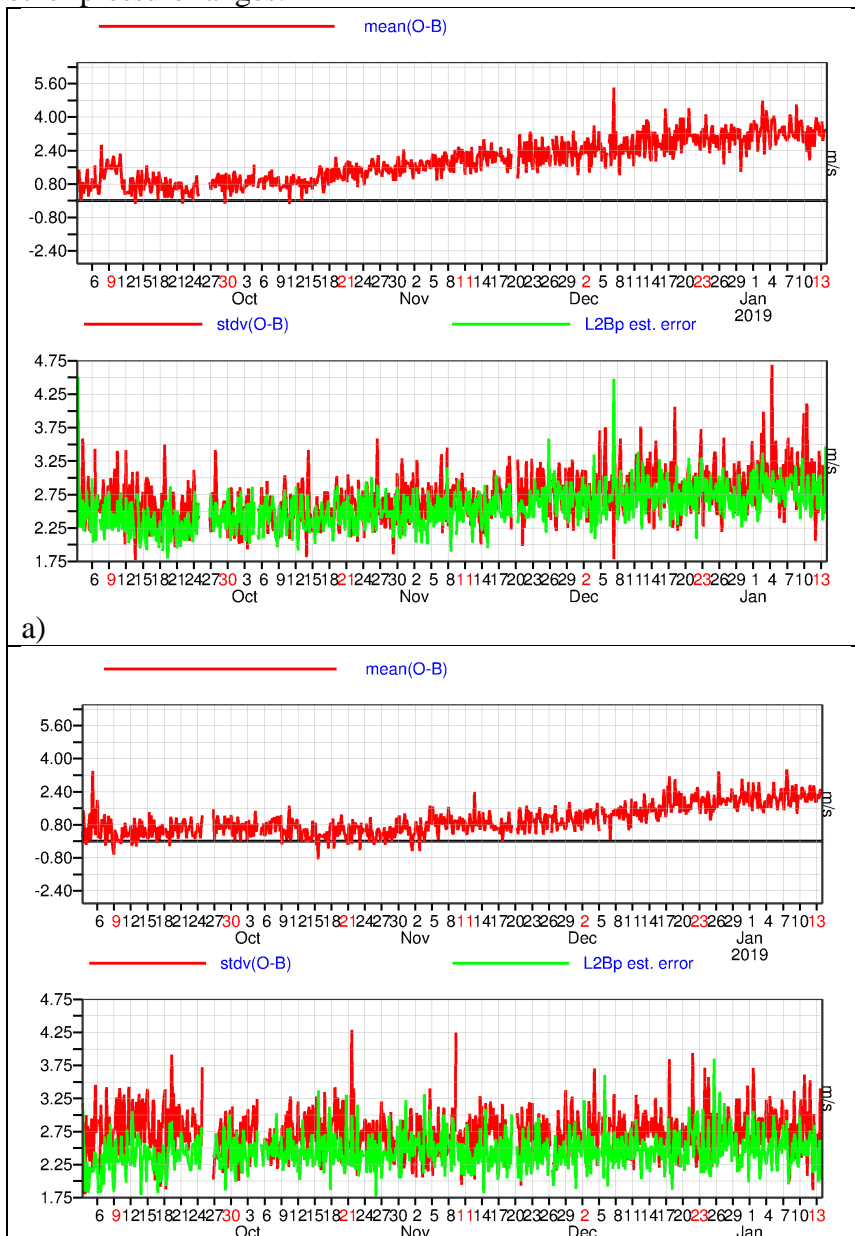
b)

Figure 8. Time series (every 4 hours) of L2B Mie-cloudy HLOS wind mean(O-B) (top plot of each figure) and stdev(O-B) (bottom plot of each figure) for the pressure range 752-867 hPa for descending orbit phases only. a) Northern hemisphere extratropics (20-90 degrees latitude) b) southern hemisphere extratropics (-20 to -90 degrees latitude). The green line is the L2Bp estimated error derived from useful signal information.

4.1.3 Comparison of data quality in mid-September 2018 to early January 2019

4.1.3.1 L2B Rayleigh-clear

ALADIN's FM-A reported laser UV energy per pulse dropped from approximately 61 mJ to 52 mJ (as can be determined from the L1B products) from 15 September 2018 (mid-September) to 10 January 2019 (early January). Plots of O-B statistics as a function of altitude for the two periods are shown in Figure 9 (using the AUX_MET method; see Section 3.2). There is a sample of around 80,000 observations in both cases (around 20 hours of data). The "robust standard deviation" in Figure 9 is the median absolute deviation (MAD) scaled by 1.4286 which is equivalent to the standard deviation for a normal distribution (Ruppert, 2010). The scaled MAD is less prone to outliers than the standard deviation, which is useful given that no first-guess check is applied in these plots.
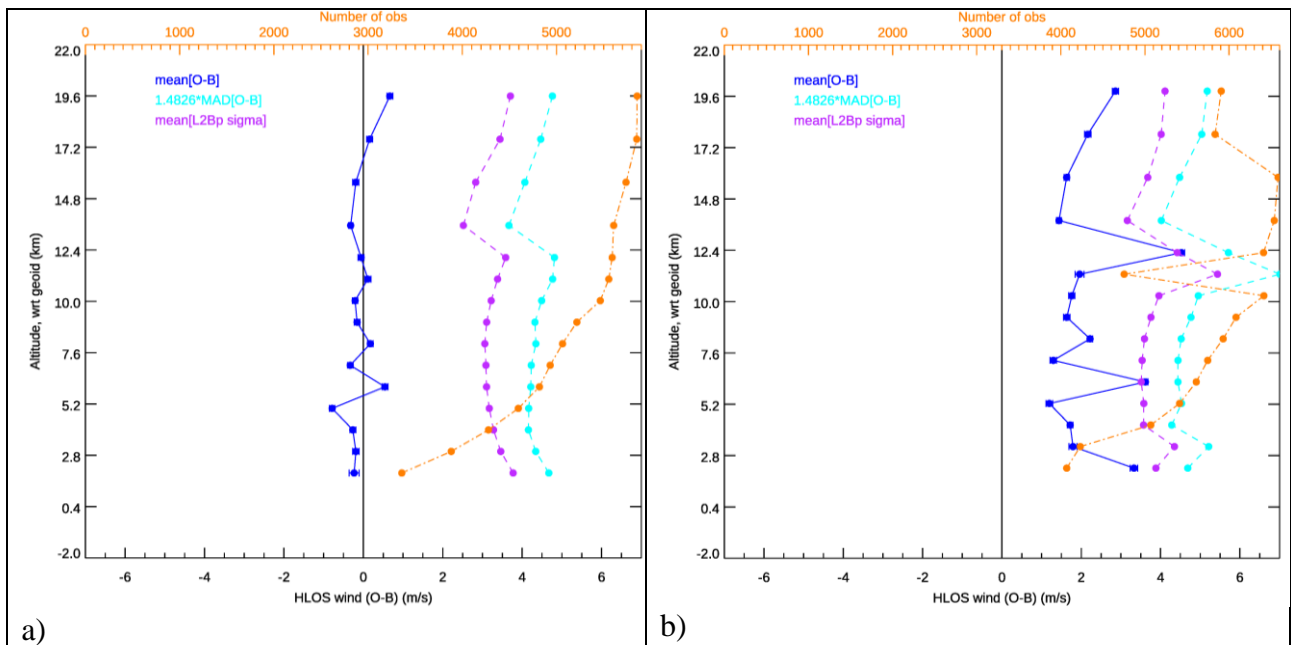

Figure 9. Global L2B Rayleigh-clear HLOS wind O-B statistics as a function of altitude. The dark blue line is the mean(O-B), the cyan line is the robust standard deviation of O-B, the purple line is the mean of the L2Bp estimated error and the orange line is the number of observations (top x axis). a) For mid-September 2018 b) for early-January 2019.

It is evident from Figure 9 that the accuracy and precision of the Rayleigh winds degraded with time during the CP. As already shown in Figure 3 and Figure 5, the Rayleigh winds were relatively unbiased in mid-September 2018 and became positively biased by early January 2019. The bias in early January 2019 shows spikes for several range-bin due the hot pixel effect mentioned earlier. The global average O-B bias in early January 2019 is about 2 m/s if the hot pixels are not considered. Given that global biases of ECMWF u-wind relative to radiosondes are rather small, at typically less than 0.3 m/s (confirmed by radiosonde O-B departure statistics), we can assume that the Aeolus Rayleigh observations account for the bias change. The profile average robust standard

21

deviation of O-B is 4.4 m/s in mid-September and 4.9 m/s in early January. Also, the counts are relatively reduced at specific range-bins in early January due to the applied 8 m/s estimated error QC rejecting more data than in September (overall 4% more rejections). Note that the L2Bp estimated random errors increase in the summer poles due to larger solar background noise estimated, and hence the QC rejections are not a strictly fair comparison.

As mentioned earlier, some of the degradation in the Rayleigh wind quality in early January 2019 is exacerbated by the L2Bp measurement-bin level classification procedure performing worse than in mid-September 2018, as the noise of the L1B scattering ratios increased due to lower laser energy. The quality loss could be mitigated to a reasonable extent by retuning the L2B processor scattering ratio classification thresholds. Increasing the scattering ratio threshold to 1.6 from 1.25 allowed an increased number of genuinely clear measurement-bins into the calculation of Rayleigh-clear winds, hence reducing the noise. Also, some improvement was obtained by rejecting huge spikes in signal levels, which are thought to be due to cosmic radiation affecting the instrument. This led to the overall O-B robust standard deviation improving by about 0.3-0.4 m/s (as is evident in Figure 4 after the 11 January 2019).

Figure 10 shows the L2B Rayleigh-clear wind quality across the dynamic range of HLOS wind for the two periods. The linear correlation coefficient for mid-September from a) is 0.96 but is reduced slightly in early January to 0.95 via b). That is, the Rayleigh winds performed well over the dynamic range in both periods. To estimate the wind speed dependent errors, we plot the mean(O-B) as a function of B in c) and d) of Figure 10. The use of "Desroziers diagnostics" (Desroziers et al., 2005) on conventional u-wind observation departures (radiosondes, aircraft) gives a global average value for the background forecast random error of $\sigma_B = 1.6$ m/s (not shown). Errors in the independent variable (in this case the background HLOS wind) of a regression scheme leads to biases in the estimated fit coefficients; for a simple linear regression, an underestimate of the fit coefficient known as attenuation bias or regression dilution occurs (Frost, 2000). Because for the Rayleigh winds σ_B is significantly less than σ_O it is reasonable to have B as the independent variable. Simulations of the attenuation bias induced by the assumed σ_B produce a slow bias of -1.5% (not shown). The linear fit coefficient in c) shows a slope error of -4% in mid-September 2018. This is significantly more negative than the -1.5% that would be expected without any real wind speed dependent biases and therefore it can be assumed to be a real Rayleigh slow bias in mid-September 2018 of approximately -2.5%. This slow bias partially accounts for the ascending/descending orbit phase bias differences in September 2018 already noted from Figure 3. The linear fit coefficient in early January from d) is around -1%, so the slope error is closer to the expected -1.5% early January than in mid-September 2018. The reason for this is that the true Rayleigh response functions changed with time such that, by chance, the slope error improved with time by continuing to use the older but incorrect CP Rayleigh calibration file.
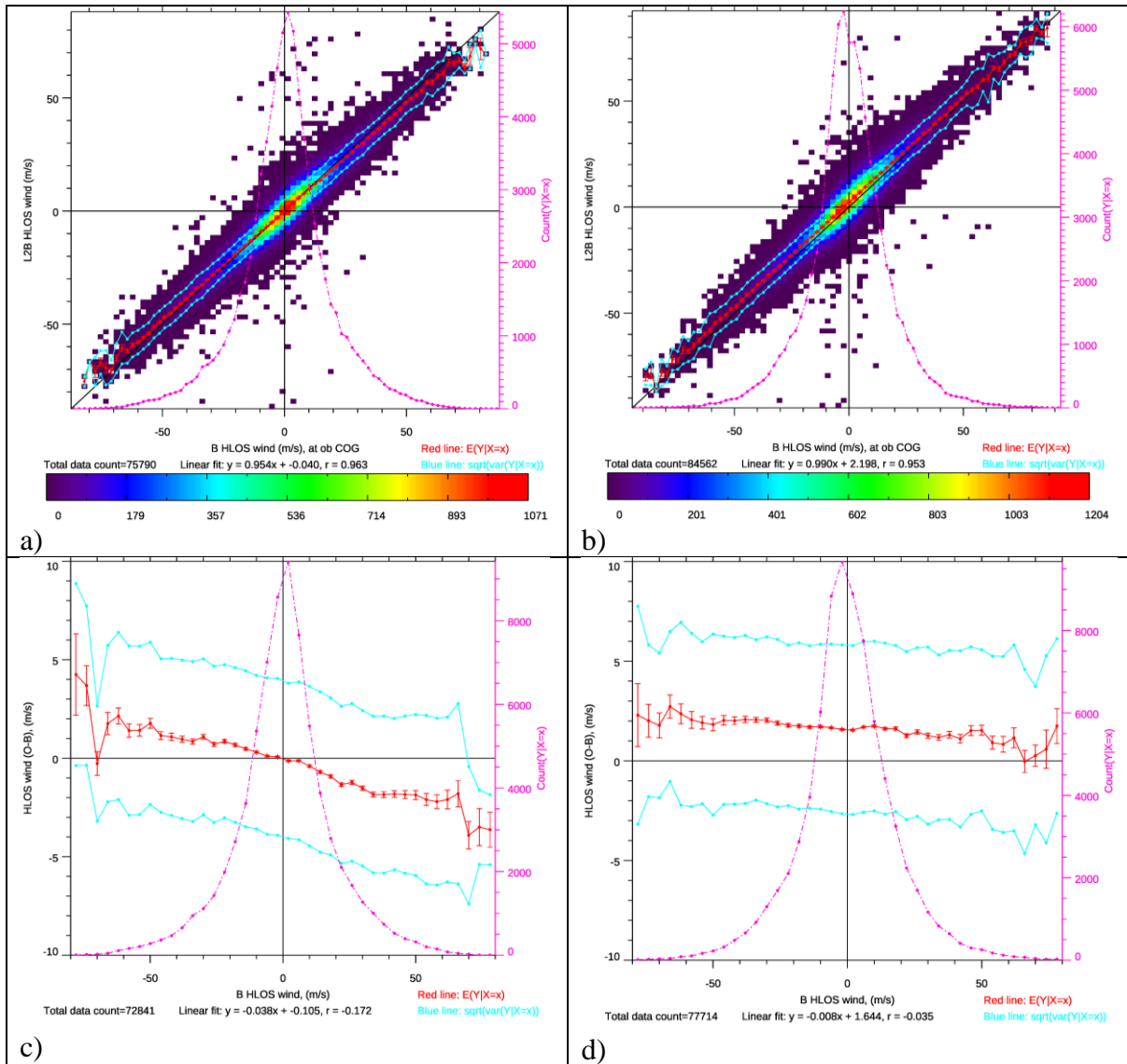
Figure 10. Global L2B Rayleigh-clear O-B statistics over the HLOS wind dynamic range. Dependence of L2B HLOS wind on background HLOS wind: a) in mid-September 2018 and b) in early-January 2019, as shown by 2D histograms. Dependence of mean(O-B) on background HLOS wind in c) mid-September 2018 and d) early-January 2019; the red-line is the mean(O-B) binned as a function of B (with the error bar showing the standard error of the mean), the cyan lines are the ± standard deviation of O-B. The pink lines are the data count.

It was discovered that the Aeolus observation bias varies along the orbit; the variation with orbital phase angle (argument of latitude) is shown in Figure 11 for the Rayleigh winds. Zero degrees argument of latitude corresponds to the ascending node equator crossing point. The descending phase of the orbit is between 90 and 270 degrees, elsewhere it is ascending. It can be seen in mid-September 2018 a), that the bias was more positive in the descending phase and more negative in the ascending phase; which concurs with the assessment of Figure 3 and Figure 10. There is also an orbital phase dependent bias in early January 2019 as shown in Figure 11 b) which peaks at the north pole and is at its minimum at the south pole. This has been shown (via L2B processor testing and personal communication with DLR) to be partially caused by an imperfect correction of the satellite LOS velocity; but for the Rayleigh this is not the dominant source. If the LOS correction is switched off in the L2B processor the bias shows less variation with orbit phase in early-January 2019 (not shown). The reported satellite velocity correction maximum amplitude was small at ~0.16 m/s HLOS in

September 2018 but was up to 1 m/s HLOS in early January with a similar sinusoidal shape as a function of argument of latitude to the mean(O-B) bias. A similar variation of the bias on argument of latitude for the Mie winds in early-January is shown in Figure 14 b); since it applies the same satellite LOS velocity correction. The cause of the imperfect satellite LOS velocity correction is being investigated by ESA and Airbus. It should also be noted that possible instrument and satellite thermal and range variability effects along the orbit are not yet corrected for in the L1B algorithm as originally intended with the so-called harmonic bias estimator based on zero-wind ground return observations. In future data reprocessing, this will be attempted and may mitigate the variable biases in the data product reported here.
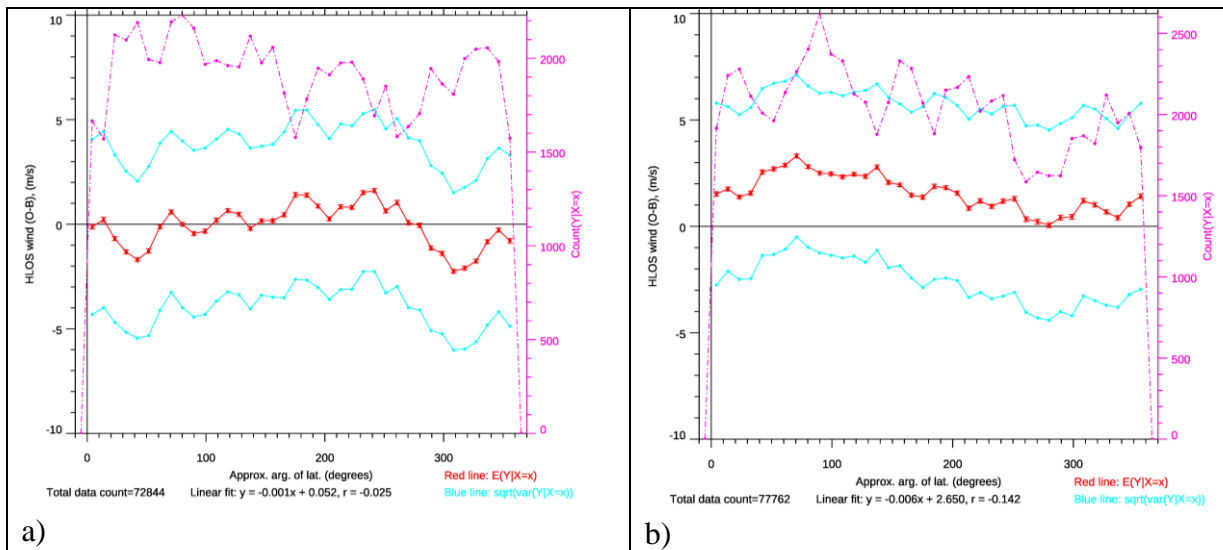

Figure 11. Dependence of the L2B Rayleigh-clear HLOS wind mean(O-B) on the orbital phase angle (argument of latitude) from zero degrees at the ascending node equator crossing point. The red-lines are the mean(O-B) binned as a function of argument of latitude (with the error bar showing the standard error of the mean), the cyan lines are the ± standard deviation of O-B and the pink line is the count.

4.1.3.2 L2B Mie-cloudy

The global L2B Mie-cloudy O-B statistics for mid-September 2018 and early January 2019 are shown in Figure 12. The average bias in mid-September 2018 was 1.2 m/s, as is also evident in Figure 6. This bias grew significantly and by early January 2019 had reached 4 m/s, after excluding the negatively biased data due to the hot pixel at roughly 3 km (range-bin 13). The Mie-cloudy random error as assessed by the L2Bp estimated error is almost identical in mid-September 2018 and early January 2019 (at 1.65 m/s), however the profile average robust standard deviation increased from 3.25 m/s to 3.49 m/s, which may be associated with the hot pixel (see the peak in robust standard deviation at ~3 km). In summary, the Mie random error is similar for the two periods and does not show an obvious effect of the laser energy decrease, as also shown in Figure 7. This is assumed to be true at least for the cloud-target Mie winds which have strong backscatter but may be less true for weaker backscatter targets.
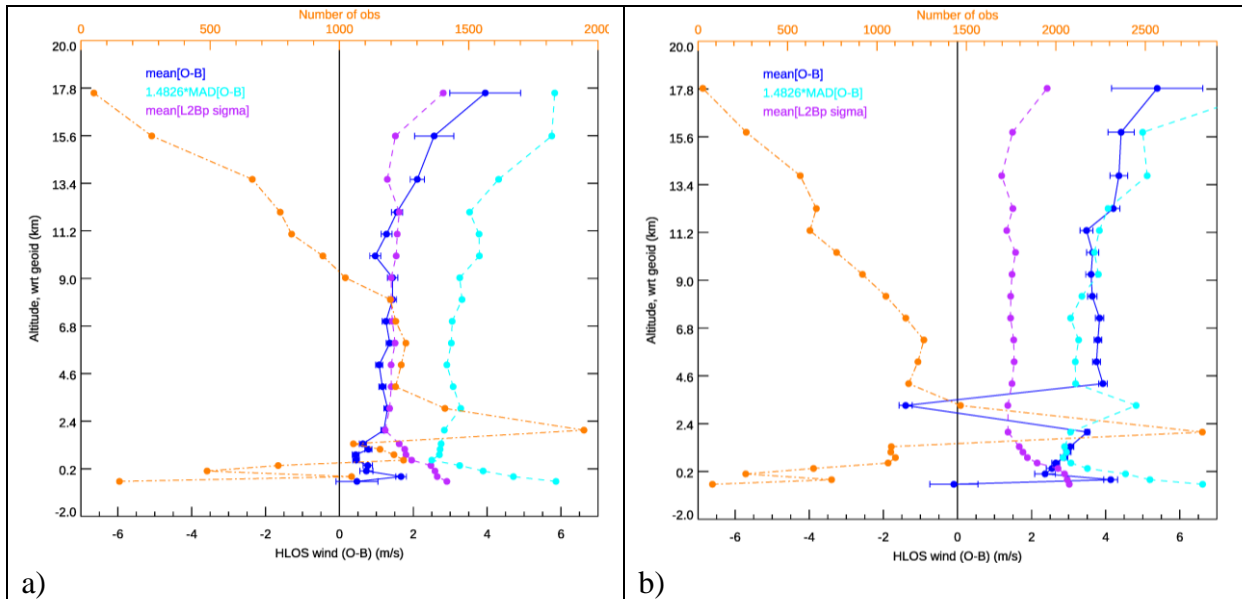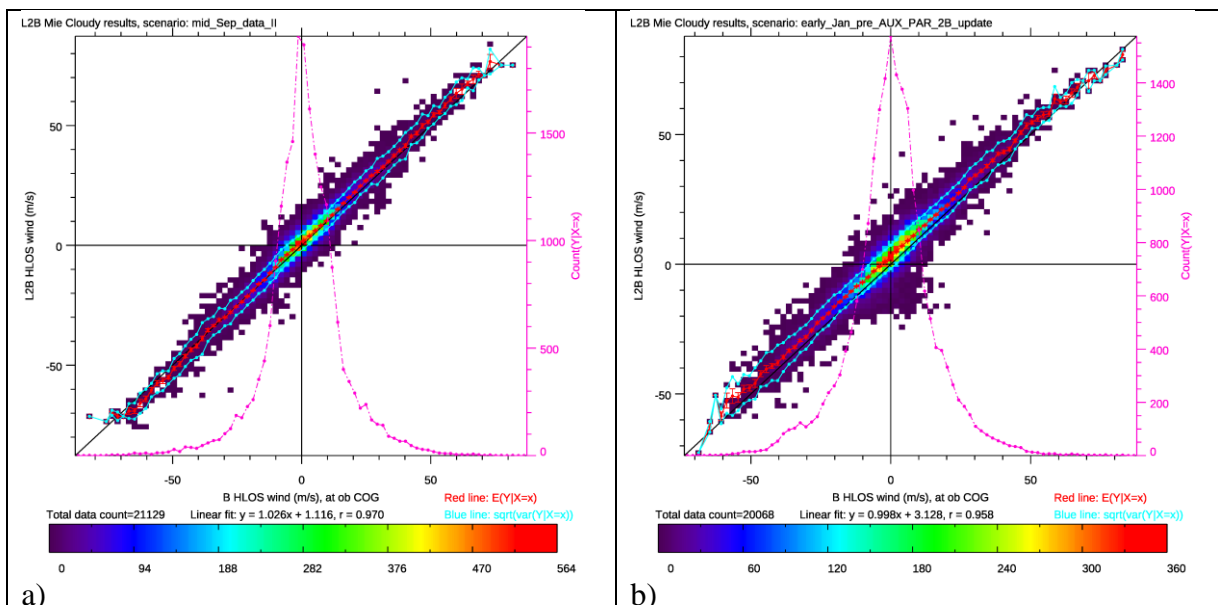
Figure 12. Global L2B Mie-cloudy HLOS wind O-B statistics as a function of altitude. The dark blue line is the mean(O-B), the cyan line is the robust standard deviation of O-B, the purple line is the mean of the L2Bp estimated error and the orange line is the number of observations (read off top axis). a) For mid-September 2018 b) for early-January 2019.

The Mie-cloudy HLOS wind quality over the dynamic range is shown in Figure 13. They have high correlation coefficients of 0.97 in mid-September a) and 0.96 in early January b). The wind speed dependent bias shows a fast bias in mid-September with a linear fit of +5%, see c). Note that the independent variable is chosen to be (O+B)/2 rather than B alone, because the Mie observation random errors are of similar magnitude to the model background errors, therefore to decrease the effect of errors in the independent variable for the regression it is useful to average them. The fast bias also occurs in early-January but is smaller at +3%, see d). It is unclear if the fast bias of the Mie observations relative to the model is a problem with the Mie calibration or in the model winds in the cloudy areas that the Mie samples. It shall also be noted hereby that the Mie winds are distributed differently in the horizontal and vertical than the Rayleigh winds, which may lead to differences in the statistics as compared to the ECMWF model background.
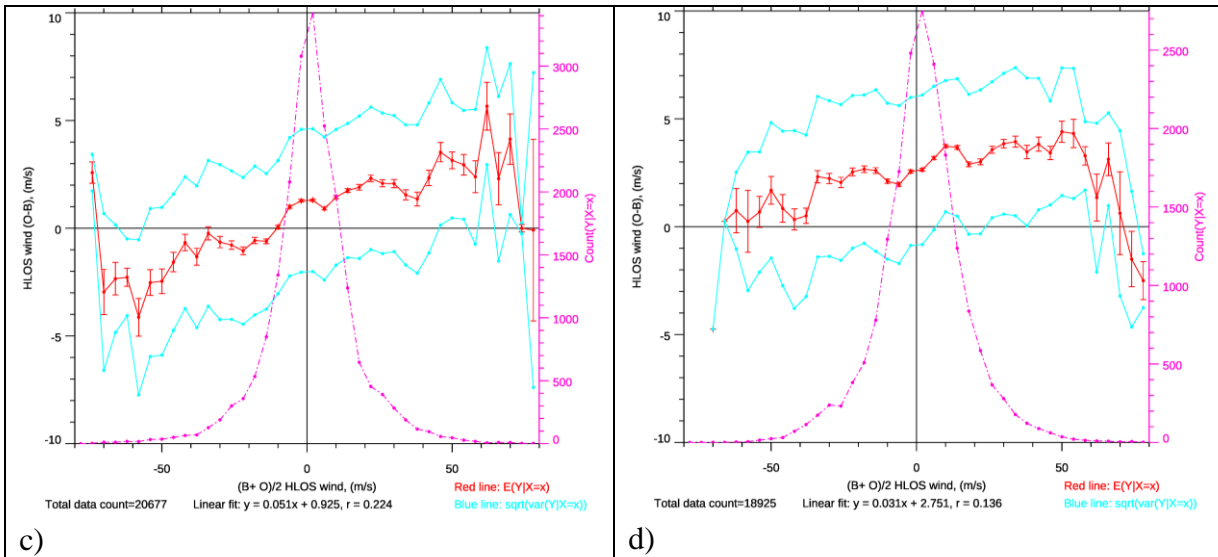
Figure 13. Global L2B Mie-cloudy O-B statistics over the HLOS wind dynamic range. Dependence of L2B HLOS wind on background HLOS wind a) in mid-September 2018 and b) in early-January 2019, as shown by 2D histograms. Dependence of mean(O-B) on background HLOS wind in c) mid-September 2018 and d) early-January 2019; the red-line is the mean(O-B) binned as a function of B (with the error bar showing the standard error of the mean), the cyan lines are the ± standard deviation of O-B.

The Mie-cloudy bias as a function of argument of latitude is shown in Figure 14. The dependence in mid-September 2018, Figure 14 a), is thought to be mostly a result of the fast bias (reported above) given the variations in the average HLOS wind along the orbit. The behaviour in early January 2019, Figure 14 b), shares a similar pattern to the applied satellite LOS velocity correction and it thought to be mostly due to this imperfect correction (as discussed earlier for the Rayleigh).
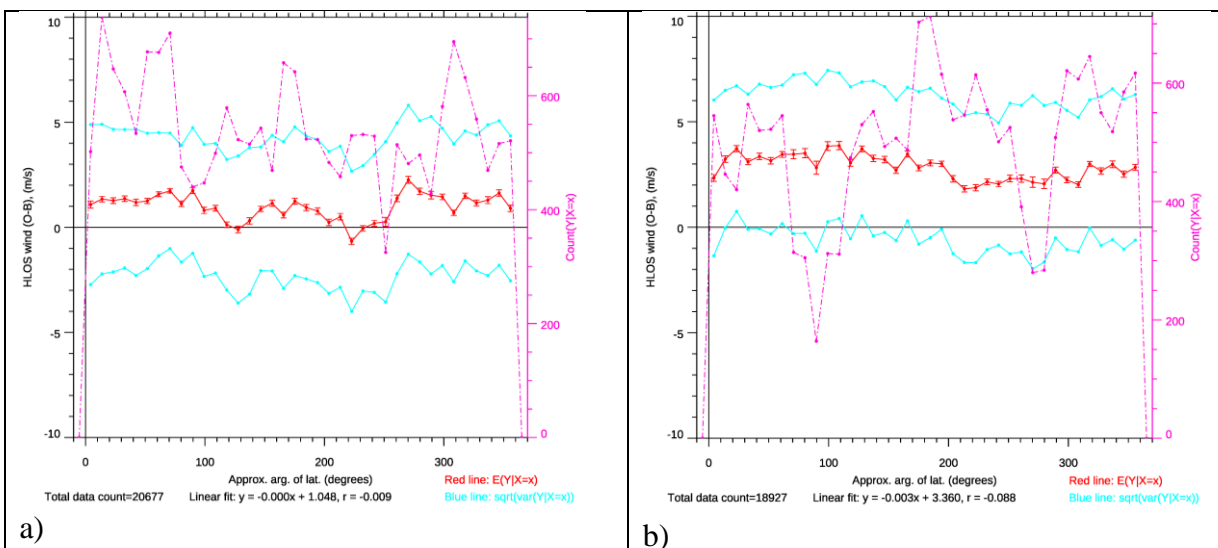

Figure 14. Dependence of the L2B Mie-cloudy HLOS wind mean(O-B) on the orbital phase angle (called argument of latitude) from zero degrees at the ascending node equator crossing point. The red-lines are the mean(O-B) binned as a function of argument of latitude (with the error bar showing the standard error of the mean), the cyan lines are the ± standard deviation of O-B and the pink line is the count.

The Rayleigh-cloudy and Mie-clear L2B O-B statistics have not been discussed. This is because they are significantly worse than the Rayleigh-clear and Mie-cloudy results in terms of biases and random

TN 18.7
An assessment of Aeolus wind observations with the
ECMWF model and preliminary Observing System
Experiments

Ref: AE-TN-ECMWF-GS-187
Version: 1.1
Date: 8 August 2019

errors.

4.1.4 Aeolus HLOS wind random and systematic error assessment

The background forecast's random error varies geographically, being largest at the tropical tropopause and smallest in the NH mid-latitudes based on ECMWF EDA spread (not shown). A global average value for the background u-wind component is estimated to be 1.6 m/s (1-σ) using "Desroziers diagnostics", see Section 4.1.3.1 (a similar number is derived for the v-component, hence this applies also for the HLOS wind component). From this estimate and our O-B standard deviations in Section 4.1.3, an approximate global average level of random error of the Aeolus L2B HLOS winds is calculated using this formula:

$$\sigma_O = \sqrt{\sigma_{O-B}^2 - \sigma_B^2}$$

This is derived using the assumption that the observation and background errors are uncorrelated. This estimate of Aeolus observation error includes the representativeness error due to mismatch between what the observation represents and what the model can represent, given, for example, the point-like observation operator.

Table 1. Estimating the global average Aeolus L2B observation error during the CP.

Observation type	Average HLOS wind O-B robust standard deviation (m/s)	Average O (1-sigma) estimate (m/s)
L2B Mie-cloudy	3.4	3.0
L2B Rayleigh-clear	4.6	4.3

The Aeolus L2B HLOS Rayleigh wind random error levels are larger than the pre-launch mission requirements (Ingmann and Straume, 2016) specified before launch, but we believe they are still good enough to demonstrate NWP impact (see Section 0). Aeolus has smaller representativeness error compared to e.g. radiosonde winds, which helps it still be useful despite the lower instrumental precision.

The systematic errors of Aeolus have been shown to vary in complex ways i.e. with time, with orbit phase, with hot pixels. The magnitude of the bias is throughout most of the CP greater than the mission requirements. This however, should be improved in the future as increasing understanding of the biases is obtained and as calibration methods are determined or improved, and finally fully applied.

27

4.2 Initial Observing System Experiment results

For the experiment using the Rayleigh-clear and Mie-cloudy (refer to as "Rayleigh+Mie", see Section 3.3.2), when Aeolus L2B winds are assimilated, the 4D-Var analysis follows expectation and is pulled towards the Aeolus L2B winds; this is shown by the statistics of observation minus analysis (O-A) relative to O-B statistics in Figure 15. The analysis at the observation geolocation pulls relatively much closer to the Mie winds compared to the Rayleigh due to the Mie's significantly smaller assigned observation errors (less than half the Rayleigh). However, there are about five times as many Rayleigh winds as Mie winds assimilated and the Rayleigh has a much greater spatial coverage of the atmosphere. These globally averaged statistics show relatively small biases (as expected during the focus period, see Section 3.3.3). However, there does appear to be some positive global average bias for upper levels for both the Mie and the Rayleigh winds, and at lower levels for the Mie winds. There is a negative bias at around 500 hPa for the Rayleigh, which is also seen in Figure 3, which is not yet understood.
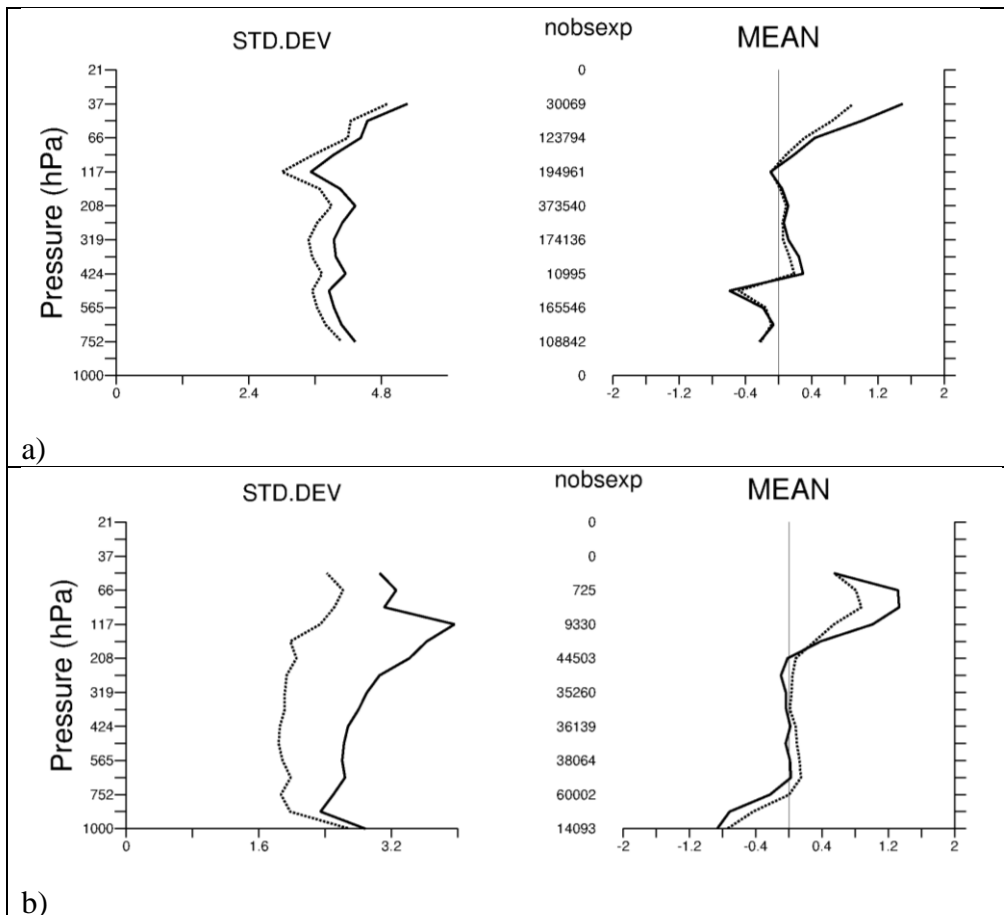

Figure 15. Global O-B (solid) and O-A (dotted) departures statistics as a function of pressure when L2B Rayleigh-clear plus Mie-cloudy HLOS winds are assimilated. The variable on the x-axis is HLOS wind (m/s). The standard deviation is shown on the left, and the mean on the right and the sample size is listed in the middle. The L2B Rayleigh-clear statistics and in a) and b) are the L2B Mie-cloudy statistics. The period is from 12/9/2018 to 16/10/2018.

Assimilating Rayleigh winds has a notable effect on the mean analysis state for the u-wind component, as shown in Figure 16 (for both a) Rayleigh+Mie and b) Mie only experiments). Note that the effect of Mie winds on mean state is much smaller. The effect is strongest in the tropics for

Rayleigh+Mie where the generally easterly winds are made stronger by approximately 0.5 m/s in the zonal average (as checked but not shown). This change leads to an increase in bias with respect to tropical radiosonde u-wind mean(O-B) (not shown), hence it is assumed to be Aeolus induced bias and not correcting a model bias. Interestingly the bias is improved against radiosonde v-wind. The systematic u-wind changes persist in the longer forecast ranges e.g. seen at day 8 forecasts.

The Rayleigh wind speed dependent slow bias (see Figure 10 c) is -2.5% for most of September, which should lead to a reduction in the tropical easterlies and not an increase. On closer inspection, it is found that for the small wind speeds found in the tropics, the descending orbit phase is positively biased relative to the ascending phase (not shown) by about 2 m/s. The descending phase bias is causing the tropical easterlies to become stronger. The cause of this bias is not yet understood; however, in the orbital phase dependence of the bias is different in January 2019. The slight decrease by 0.03 m/s in the polar vortex (polar night jet) in the SH, is thought to be due to the Rayleigh slow bias as shown in Figure 10 c).
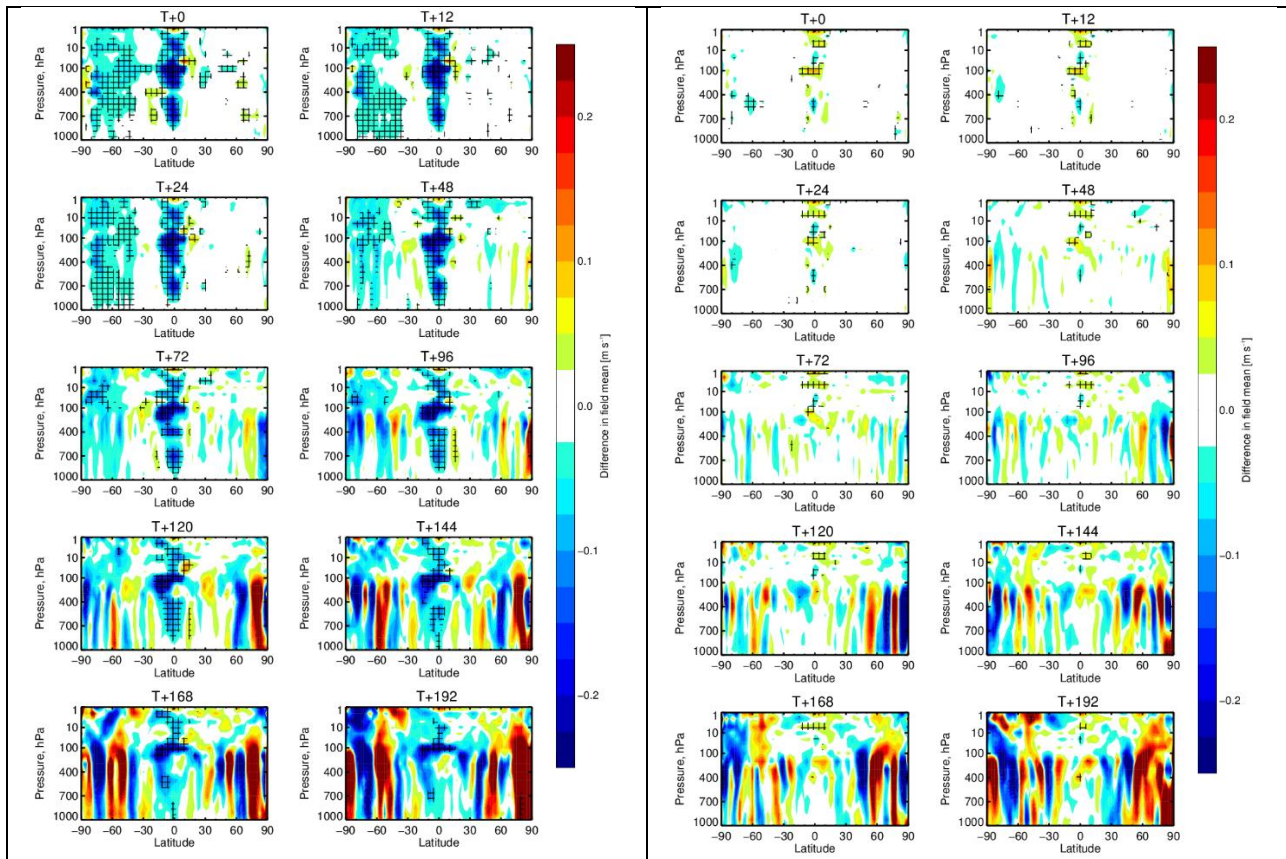

Figure 16. The zonal mean change in analysis (T+0 hours) and forecast (T+12 to T+192 hours) u-wind fields resulting from assimilating a) L2B Rayleigh-clear and Mie-cloudy HLOS winds and b) L2B Mie-cloudy winds only.

The impact of Aeolus for this relatively short OSE is most robustly demonstrated in the short-range forecasts (up to 12-hour forecasts), via the change in fit of the forecasts to other assimilated observation types; this is shown in Figure 17. The other observation types consist of: conventional wind observations (radiosondes, pilots, aircraft and radar wind profilers); AMSR-2 (Advanced Microwave Scanning Radiometer 2) all sky radiances; radiosonde temperature; aircraft temperature; geostationary satellite radiances; GPSRO (Global Positioning System radio occultation) and AMSU-A (Advanced Microwave Sounding Unit-A) radiances (mostly temperature information). For the Rayleigh+Mie experiment, the fit to conventional wind observations (which is dominated by the very

large sample of aircraft wind observations) shows an improvement of around 1% in the SH at 300 hPa (~8 km). The improvement in the tropics is roughly 0.7%, with only a small improvement evident in the NH. Note that the fit to u and v-winds from radiosondes only (not shown) is larger e.g. up to 1% in the NH, 2% in the tropics and 1% in the SH; perhaps because aircraft follow very similarly geolocated flight paths means that the forecast winds are much better in those areas. The assimilation of only the Mie winds (red lines) seems to provide a reasonable fraction of the Rayleigh+Mie impact (black lines). Wind improvements of order 1% in SH and tropics may not sound to those unfamiliar with such statistics as particularly impressive, but they are comparable to the impact of other satellite observation types such as infrared sounders, AMV (atmospheric motion vectors) or GPSRO in troposphere as shown in recent ECMWF OSE denial experiments (Bormann et al., 2019).

Globally it is seen that the fit to radiosonde and aircraft temperatures is improved by 0.5% at 300-400 hPa. The fit to GPSRO is improved by 0.8% at 11 km. In terms of humidity and cloud information there is an improvement of 0.8% against some channels of AMSR-2 and improvements in other humidity sensitive observations such as e.g. MHS (Microwave Humidity Sounder), geostationary infrared imagery. The only observation type to show a clear degradation are the microwave temperature sounders in the lower stratosphere i.e. AMSU-A and ATMS (Advanced Technology Microwave Sounder). AMSU-A channel 11, which peaks around 25 km, shows the worst degradation, but note that Aeolus provided winds only up to around 20 km altitude for this period, hence the degradation does not seem to be the direct effect of its assimilation. Interestingly it must be the Rayleigh winds that cause this degradation, because the Mie only experiment does not show the negative impact against AMSU-A.
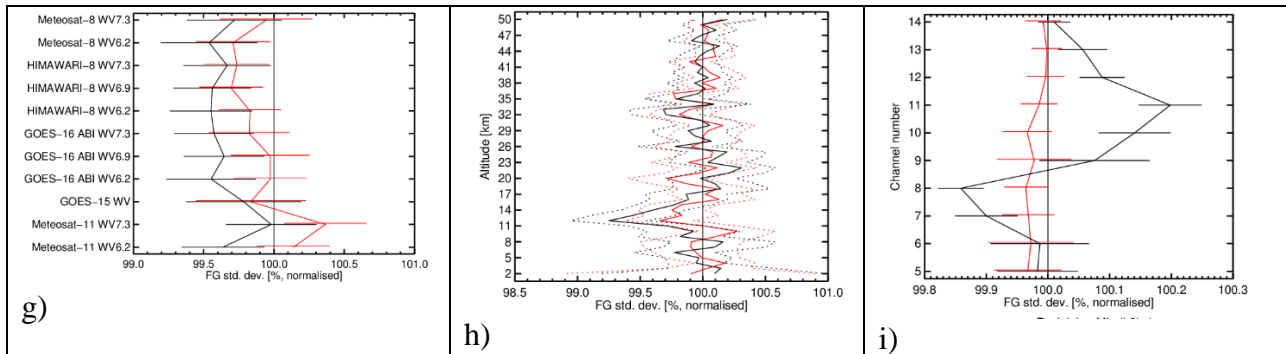

a) b) c)
d) e) f)
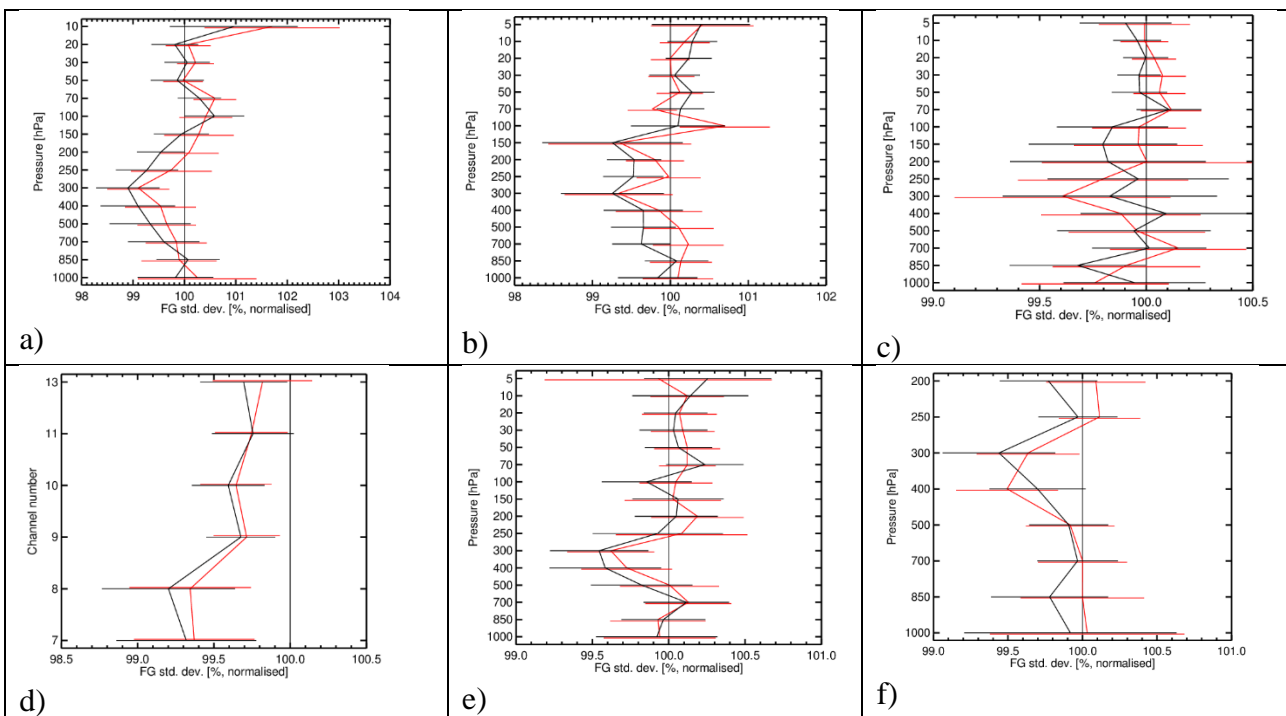
Figure 17. Change in standard deviation of O-B departures resulting from assimilating Aeolus HLOS wind observations, normalised so that the control is 100%. Values below 100% show an improved fit from assimilating Aeolus and above 100% show a degraded fit. The observation types are a) conventional vector wind in the SH extratropics, b) conventional vector wind in the tropics, c) conventional vector wind in the NH extratropics, d) global AMSR-2 all sky radiances, e) global radiosonde temperature, f) global aircraft temperature, g) global geostationary satellite radiances, h) global GPSRO bending angle and i) global AMSU-A radiances. The black lines are the Rayleigh+Mie experiment and the red lines are the Mie only experiment. Horizontal bars show the 95% confidence range.

The impact of Aeolus on the longer forecast ranges as verified against own analyses is shown in Figure 18 (both experiments) and Figure 19 (the Rayleigh+Mie experiment only). There are hints of positive impact for the Rayleigh+Mie experiment in the SH at longer forecast ranges of order 2%; and in the tropics at higher altitudes. The impact on the 500 hPa geopotential heights in the SH also looks promising (not shown). However, the confidence intervals suggest the impact is mostly not statistically significant. A larger reprocessed L2B dataset without bias drift (e.g. six months) would allow for a more robust assessment of the longer-range forecast impact. The impact of the Mie only experiment looks to be neutral, as can be seen in Figure 18, in contrast to the short-range forecast fit to other observation types; this result is not yet understood. The apparent degradation in the shorter range forecasts (red areas in Figure 19) is a typical feature of verification against own analyses when adding a new observation type which adds variability to the forecasts, and given the improved fit of short-range forecasts to other observation types it is not of great concern.
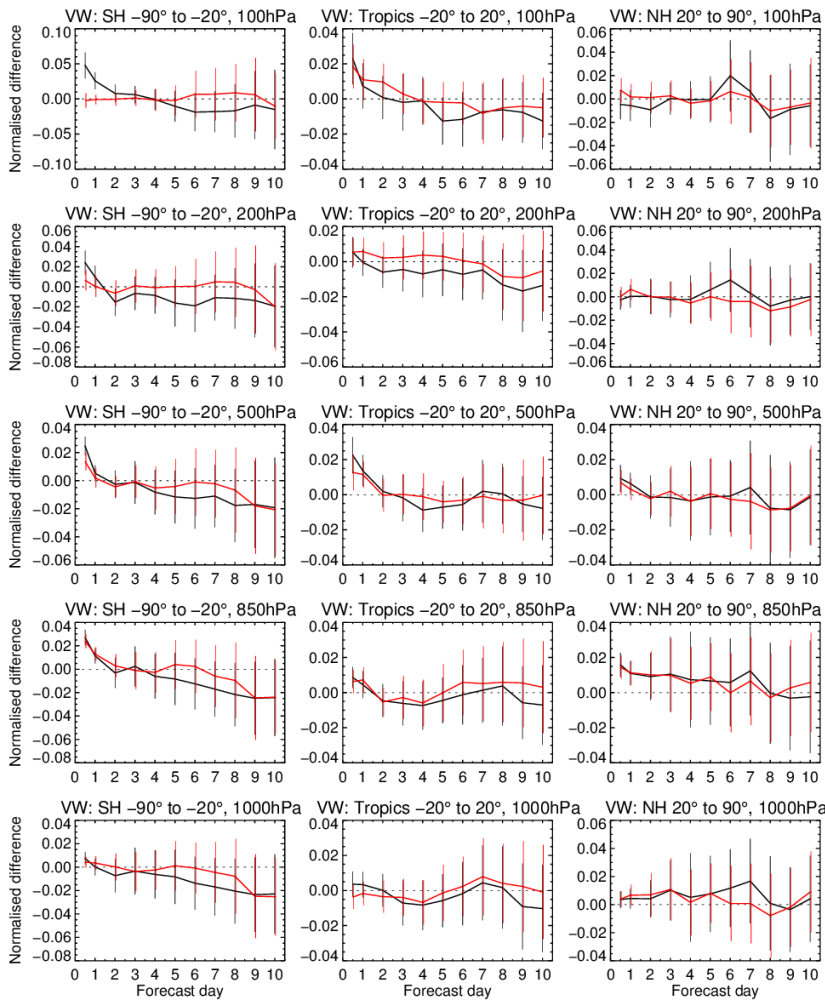
Figure 18. Normalised change in the RMS (root mean square) error in wind vector for different vertical levels (from 100 to 1000 hPa, top to bottom) and for SH, tropics and NH (left to right). The black line is for the Rayleigh plus Mie experiment and the red line is for the Mie only experiment. The period is from 12/9/2018 to 16/10/2018. Confidence range are 95%. Negative values indicate a reduction in error from assimilating Aeolus.
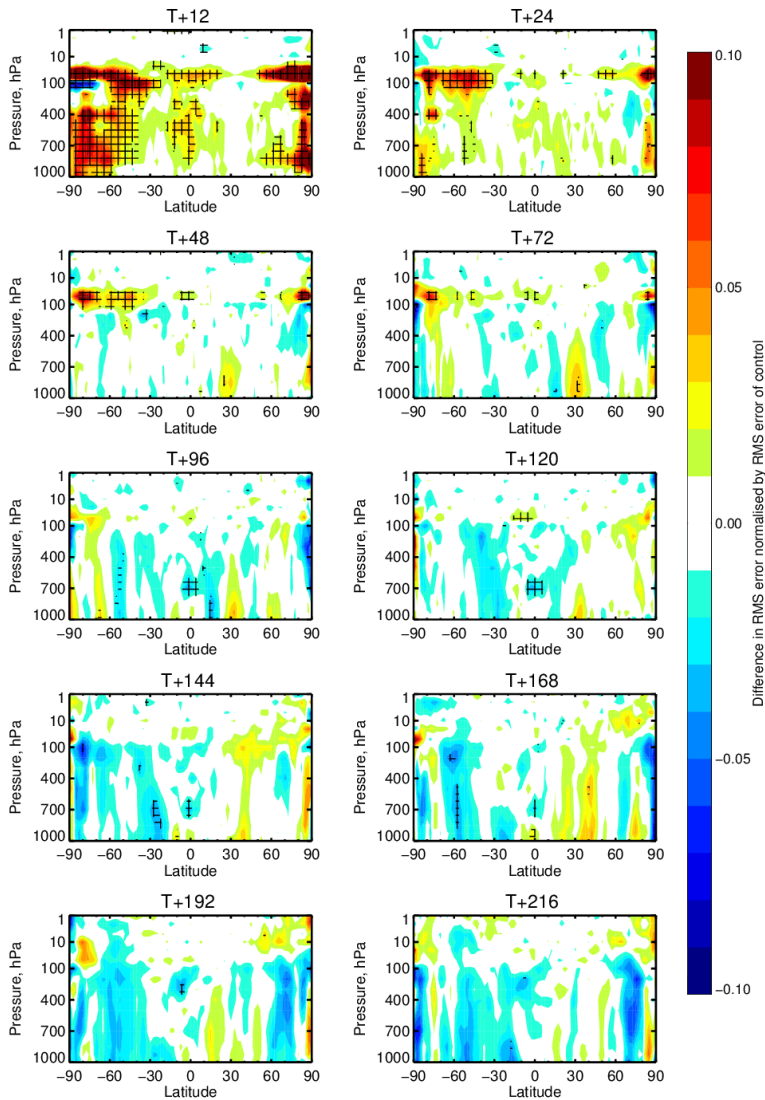
Figure 19. Zonal average normalised change in the RMS (root mean square) error in wind vector for the Rayleigh plus Mie experiment for the period 12/9/2018 to 16/10/2018. Negative values (blue) indicate a reduction in error from assimilating Aeolus and red values an increase in error.

5 Discussion

We determined a precision of approximately 4.3 m/s and 3.0 m/s for the L2B Rayleigh-clear and Mie-cloudy HLOS winds respectively. The bias (accuracy) is more variable with time (due in part to the static calibration strategy for the CP data processing) but certainly reaches levels of 2 m/s for much of the CP. The precision and accuracy of the Aeolus L2B winds can be compared to ESA's mission requirements (Ingmann and Straume, 2016), which are 2.5 m/s in the free troposphere and biases less than 0.7 m/s. Hence, the L2B Rayleigh-clear HLOS winds have random and systematic errors larger than the mission requirements. DLR's investigations (personal communication) show that the atmospheric path Rayleigh signal is around 2.7 times lower than expected, which when considering only shot-noise effects would make the Rayleigh wind random errors approximately 64% larger than otherwise. Such a scaling factor would lead to 2.5*1.64=4.1 m/s which is in approximate agreement with our precision estimate. The cause of the lower than expected signal levels is still being investigated by ESA and Airbus and will not be discussed here. The L2B Mie-cloudy random error estimates are closer to the mission requirements in the free troposphere (at least for strong backscatter

(cloud) targets which predominate) and given the uncertainty in the assumed background random error estimate and representativeness error, we cannot be certain if they do or do not meet them. However, the systematic error requirements are certainly not yet met for the Mie channel in the CP dataset; given the applied 1.35 m/s bias in September-October 2018 period and increasing bias thereafter (again partly due to a static calibration strategy).

There is potential to meet the requirements for systematic errors for both channels as our knowledge of the instrumental drift mechanisms improves, calibration processing software is improved and when strategies to apply the zero-wind reference ground-returns in bias correction procedures are achieved. Despite the higher Rayleigh random errors, the continuous nature of the Aeolus observations along the orbit track leads to some redundancy, hence larger random errors are probably not as damaging as they could be if the profiles were all very well separated in space and time. It should also be noted that a potential error correlation for adjacent Aeolus observations are expected to be small (Ingmann and Straume, 2016). Also, the continued lack of wind profiles in ocean areas particularly in SH, still gives the potential for impact, despite the increased noise.

Horányi et al. (2015b) showed using the ECMWF system that when assimilating real HLOS winds derived from conventional wind observations, biases that are a large fraction of the standard deviation of observation error lead to all the positive impact being lost, and with large enough bias an overall negative impact results. To try to avoid negative impact, we chose to limit the OSE test period to a focus period of 40 days when the biases looked reasonably stable with time (and could be reasonably corrected). However, in hindsight, looking in more detail, as shown in Section 4.1, there are complex biases even in the focus period e.g. wind speed dependent and orbit phase dependent biases. The OSE ran beyond mid-October and this confirmed our expectations, in that the medium range forecast impact gradually reduced as the experiment period is extended beyond 16 October 2018 (not shown) and hence the bias grew larger; however, the short-range fits to other observations still show positive impact, but with smaller amplitude.

To use the whole CP dataset (over 4 months) in an OSE, requires the generation of a contiguous set of wind calibration data on a to be determined time period, using the most up-to-date ISR, IRC and zero wind correction (ground return) data. With the bulk of the biases removed we expect to be able to achieve a statistically significant positive impact with Aeolus for medium-range NWP.

Should the residual biases remain too large after the full instrument calibration has been applied (i.e. a significant fraction of the random error), then an option would be to apply bias correction to the model for Aeolus data in the ECMWF data assimilation. A bias model consisting of a constant term, a wind speed dependent term, and perhaps and some harmonic functional dependence on argument of latitude (orbit phase angle) may be a reasonable starting point. It may be necessary to avoid the Tropical UTLS for the predictor estimation, since wind model errors can occasionally be very large (Podglagen, 2014).

A surprise from this first Aeolus OSE was that the largest impact occurs in the Southern Hemisphere rather than in the tropics. The tropics was expected to be where Aeolus winds would provide the largest impact, due dynamical arguments suggesting the importance of wind versus mass information due to the large tropical Rossby radius of deformation. This was also the expectation given the results using real wind observations in Horányi et al. (2015a). A reason for this discrepancy may be because the referenced study added HLOS winds (derived from conventional winds) into a system starved on all conventional winds, and perhaps being the first directly measured wind profile data into a system, it gives a much larger impact than the next addition i.e. real Aeolus. This could be tested in the future by using a control without convectional winds in the tropics to see if the real Aeolus impact goes up significantly. Also, the reference could not simulate the potential Southern Hemisphere impact of Aeolus in areas which already lacked conventional winds.

However, perhaps a more important contributor is that in the tropics in September 2018, the

Rayleigh winds in the descending orbit phase had a bias of around 1-2 m/s, whereas the bias in the ascending phase was small, as shown in Figure 11 a). This increased the strength of the on average easterly tropical winds, as indicated in Figure 16. The O-B bias was increased relative to tropical radiosonde zonal winds in the focus period (not shown). This bias is a strong candidate to explain the lower than expected tropical impact.

Another potential contributor to the lower tropical impact than expected, could perhaps be related to the poorer fit to AMSU-A lower stratospheric temperature information channels in the tropics. We expected that winds would have most impact in the tropical upper-troposphere/lower-stratosphere (UTLS), an area which typically has large vertical wind shear. Perhaps the CP range-bin settings, i.e.2 km thick in the UTLS, caused problems given that they are assimilated as point winds which may have created dubious increments. Ways to mitigate this is include: improving the observation operator to a vertically averaging one, blacklist 2 km bins, or for the future to move to more NWP suitable range-bin settings i.e. 1 km thick-range-bins[5]. The negative impact against AMSU-A occurred due to the Rayleigh winds, rather than the Mie winds, as confirmed in Figure 17, perhaps because there is a much larger sample of 2 km thick Rayleigh wind results than Mie in the mostly clear air of the UTLS. A short OSE (not shown) in the April 2019 period with the new range-bin settings does not show the AMSU-A degradation in the UTLS, therefore supporting our hypothesis.

Another possible explanation for the degraded AMSU-A UTLS fit could be that the biases of the Aeolus Rayleigh winds change the mean zonal winds in the troposphere such that the model's gravity waves propagate differently and erroneously, leading to a worse fit to the truth in the lower stratosphere.

The September-October 2018 Aeolus OSE showed a consistent improvement in the fit of the short-range forecasts to humidity sounding radiance measurements, presumably because improved winds lead to the more accurate advection of humidity. This is the reverse effect to that described for the All-sky radiance assimilation results (Geer et al., 2018), in which assimilation of humidity sensitive observations during the 4D-Var window leads to the model incrementing the wind field at the start of the window such that the humidity is advected better to improve the fit to humidity sensitive observations.

The relative impact of Aeolus on the short-range can be qualitatively compared to OSE denial experiments (Bormann et al., 2019). Aeolus' 1% short-range forecast wind fit is similar in magnitude to that determined for GPSRO, infrared radiances and AMVs, which can be considered a nice result for Aeolus since it only provides 0.2% of the observations assimilated; suggesting that the impact per observation of Aeolus is high.

In future, the NWP impact could be improved via a variety of Aeolus ground segment processing improvements. For example:

- Increase the number of Mie winds via reducing the grouping length-scale. This has been shown to lead to only a modest increase in random error, yet to increase the number of Mie observation by a factor 2-3.

- A correction of the hot-pixel dark current offsets in the L1B processing step, which will reduce biases and avoid having to discard specific range-bins.

- Better classification of Rayleigh measurement-bins into clear and cloudy, so that fewer are erroneously classified as cloudy and hence signal is wasted for the Rayleigh-clear winds.

- An improved use of Mie backscatter signal on the Rayleigh channel, should allow for better quality Rayleigh-cloudy winds and hence more observations.

---

[5] More favourable UTLS 1 km thick range-bin settings became the default on 26 February 2019

- More favourable vertical sampling (range-bin settings) for NWP impact

Also, there are very likely to be several improvements possible for the data assimilation, e.g. better assigned observation errors, a vertical averaging observation operator, spatial thinning (e.g. over poles if necessary), better QC decisions.

In summary, Aeolus has demonstrated the ability to measure winds from space via the Doppler wind lidar technique. The winds so far are noisier than hoped for, but despite this they still show promise for improving weather forecasts. The observations are also more biased than required, which meant that only a few short impact experiments could be done so far. However, this is expected to be improved upon soon with the improvement of the currently applied calibrations. With future improvements in ground processing and calibration and hopefully a better performance from the second laser (FM-B) there is much to be optimistic about.

6 Conclusions

Aeolus is the first Doppler wind lidar in space. We have demonstrated, via comparisons to ECMWF's high-quality NWP model winds, that ALADIN on-board Aeolus is producing acceptable wind measurements. The estimated precision of Aeolus Level-2B HLOS winds during the Aeolus CP is approximately 4.3 m/s for the Rayleigh-clear and 3.0 m/s for the Mie-cloudy. This is less accurate than the requirements specified pre-launch for the Rayleigh channel, but is still allowing for a useful level of information content.

The biases during the Aeolus CP have been shown to vary in a much complex manner and took longer to characterize and calibrate out than expected. Also, unexpected product biases from so-called hot pixels occurred. However, there is increasing evidence that applying the detector response calibrations regularly and the ground returns for zero-wind correction should reduce the bias and bias trends to a level acceptable for NWP. This should lead to a much better reprocessed dataset soon.

Initial NWP impact experiments (OSEs) show a positive impact for Aeolus measured via the improved background departures relative to many other observation types. This shows that the short-range forecast improves when Aeolus data is assimilated. The improvements are seen for wind, temperature and humidity sensitive observations. An exception is the degraded fit to lower stratospheric satellite temperature sensitive measurements (AMSU-A and ATMS). This has been identified to be related to the Rayleigh winds assimilation and is likely due to the 2 km thick range-bins not being used properly in data assimilation, i.e. assumed to be point measurements.

Aeolus' impact on short-range forecasts is of a similar magnitude to other important satellite observing systems at ECMWF and therefore for an early impact assessment, the results look rather promising. The impact will surely increase when the biases have been reduced via reprocessing activities and as the ground segment processing algorithms and data assimilation assimilation algorithms improve. A limitation of the OSE is the short time period due to the need to avoid periods of larger and time varying biases. Ideally it should be run for much longer e.g. six months; this will be possible when the first reprocessed dataset becomes available (to be determined when) or when the near real time data processing is improved. The reprocessed dataset will have much better calibration information, leading to significantly smaller biases and bias drift.

Already from these preliminary Aeolus results it looks like Doppler wind lidars in space would be a useful addition to the global observing system and hence should be considered as part of future operational satellite missions for weather.

7 Acknowledgements

8 References

- Baker, WE, Atlas, RM, Cardinali, C, Clement, A, Emmitt, GD, Gentry, BM, Hardesty, RM, Källén, E, Kavaya, MJ, Langland, R, Ma, Z, Masutani, M, McCarty, W, Pierce, RB, Pu, Z, Riishøjgaard, LP, Ryan, J, Tucker, S, Weissmann, M, Yoe, JG. 2014. Lidar-measured wind profiles: the missing link in the global observing system. Bulletin of the American Meteorological Society 95: 4: 543– 564,

- Bormann, N., H. Lawrence and J. Farnan, 2019: Global observing system experiments in the ECMWF assimilation system, ECMWF technical Memorandum, 839

- Desroziers, G., Berre, L., Chapnik, B. and P. Poli, 2005: Diagnostics of observation, background and analysis-error statistics in observation space. Q. J. R. Meteorol. Soc. , 131, 3385-3396.

- ECMWF, 2018: IFS Documentation CY45R1. Available from ECMWF https://www.ecmwf.int/en/forecasts/documentation-and-support/changes-ecmwf-model/ifs-documentation

- ESA, 2008: "ADM-Aeolus Science Report", SP-1311,'ADM-Aeolus', April 2008, ISBN 978-92-9221-404-3, ISSN 0379-6566, 130 pp, available at https://earth.esa.int/documents/10174/1590943/AEOL002.pdf

- P. Ingmann and A.G. Straume, 2016: ADM-Aeolus Mission Requirements Document, November 216, AE-RP-ESA-SY-001

- ESA, 2019: "The Living Planet Programme", available at https://www.esa.int/Our_Activities/Observing_the_Earth/The_Living_Planet_Programme

- Frost, C. and S. Thompson (2000). "Correcting for regression dilution bias: comparison of methods for a single predictor variable." Journal of the Royal Statistical Society Series A 163: 173–190.

- Geer, A. J., K. Lonitz, P. Weston, M. Kazumori, K. Okamoto, Y. Zhu, E. H. Liu, A. Collard, W. Bell, S. Migliorini, P. Chambon, N. Fourrié, M-J Kim, C. Köpken-Watts, C. Schraff, 2018: All-sky satellite data assimilation at operational weather forecasting centres. Q. J. R. Meteorol. Soc., 144, 1191-1217. https://doi.org/10.1002/qj.3202

- Hollingsworth, A., D.B. Shaw, P. Lönnberg, L. Illari, K. Arpe, and A.J. Simmons, 1986: Monitoring of Observation and Analysis Quality by a Data Assimilation System. Mon. Wea. Rev., 114, 861–879, https://doi.org/10.1175/1520-0493(1986)114

- Horányi, A., Cardinali, C., Rennie, M. and Isaksen, L. (2015a) The assimilation of horizontal line-of-sight wind information into the ECMWF data assimilation and forecasting system. Part I: the assessment of wind impact. Quarterly Journal of the Royal Meteorological Society, 141, 1223– 1232. https://doi.org/10.1002/qj.2430

- Horányi, A., Cardinali, C., Rennie, M. and Isaksen, L. (2015b) The assimilation of horizontal line-of-sight wind information into the ECMWF data assimilation and forecasting system. Part II: The impact of degraded wind observations. Quarterly Journal of the Royal Meteorological Society, 141, 1233– 1243. https://doi.org/10.1002/qj.2551

- Illingworth, A. J., Battaglia, A., Bradford, J., Forsythe, M., Joe, P., Kollias, P., Lean, K., Lori, M., Mahfouf, J.-F., Mello, S., Midthassel, R., Munro, Y., Nicol, J., Potthast, R., Rennie, M., Stein, T. H. M., Tanelli, S., Tridon, F., Walden, C. J. and Wolde, M. (2018) WIVERN: A new satellite concept to provide global in-cloud winds, precipitation and cloud properties. Bulletin of the American Meteorological Society, 99 (8). pp. 1669-1687. ISSN 1520-0477

- Isaksen, L, Bonavita, M, Buizza, R, Fisher, M, Haseler, J, Leutbecher, M and L. Raynaud, 2010: Ensemble of data assimilations at ECMWF. ECMWF Technical Memorandum 646. Available from ECMWF https://www.ecmwf.int/en/elibrary

- Järvinen, H., Andersson, E. and F. Bouttier, 1999: Variational assimilation of time sequences of surface observations with serially correlated errors. Tellus A, 51, Issue4, 469-488.

- Q. Lu, W. Bell, P. Bauer, N. Bormann, and C. Peubey. Characterizing the FY-3A microwave temperature sounder using the ECMWF model. J. Atmos. Oceanic Technol., 28:1373–1389, 2011a.

- Ma, Z, Riishøjgaard, LP, Masutani, M, Woollen, JS, Emmitt, GD. 2015. Impact of different satellite wind Lidar telescope configurations on NCEP GFS forecast skill in observing system simulation experiments. Journal of Atmospheric and Oceanic Technology 32: 3: 478– 495,

- Marseille, GJ, Stoffelen, A, Barkmeijer, J. 2008. Impact assessment of prospective space-borne Doppler wind lidar observation scenarios. Tellus A 60: 234– 248,

- Podglajen, A., Hertzog, A., Plougonven, R. and N. Žagar, 2014: Assessment of the accuracy of (re)analyses in the equatorial lower stratosphere. J.Geoph.Res., 119, Issue19, 11,166-11,188. https://doi.org/10.1002/2014JD021849

- Rennie, M. (2016): Advanced monitoring of Aeolus winds, ESA Technical Note 16, AE-TN-ECMWF-GS-16, v1.3

- Ruppert, D. (2010). Statistics and Data Analysis for Financial Engineering. Springer. p. 118. ISBN 9781441977878. Retrieved 2015-08-27

- Stoffelen, A., 1999: A Simple Method for Calibration of a Scatterometer over the Ocean. J. Atmos. Oceanic Technol., 16, 275–282, https://doi.org/10.1175/1520-0426(1999)016

- Stoffelen, A, Marseille, GJ, Bouttier, F, Vasiljevic, D, de Haan, S, Cardinali, C. 2006. ADM-Aeolus Doppler wind lidar observing system simulation experiment. Quarterly Journal of the Royal Meteorological Society 132: 1927– 1947, https://doi.org/10.1256/qj.05.83.

- Tan, DGH, Andersson, E, Fisher, M, Isaksen, L. 2007. Observing-system impact assessment using a data assimilation ensemble technique: application to the ADM-Aeolus wind profiling mission. Quarterly Journal of the Royal Meteorological Society 133: 381– 390, https://doi.org/10.1002/qj.43

- Tan, DGH, Andersson, E, De Kloe, J, Marseille, GJ, Stoffelen, A, Poli, P, Denneulin, ML, Dabas, A, Huber, D, Reitebuch, O, Flamant, P, Le Rille, O, Nett, H. 2008. The ADM-Aeolus wind retrieval algorithms. Tellus A 60: 2: 191– 205, https://doi.org/10.1111/j.1600-0870.2007.00285.x.

- Weissmann, M., and C. Cardinali, 2007: Impact of airborne Doppler lidar observations on ECMWF forecasts. Quart. J. Roy. Meteor. Soc., 133, 107–116.

- WMO, 2018: "Rolling Review of Requirements and Statements of Guidance", available at http://www.wmo.int/pages/prog/www/OSY/GOS-RRR.html